Modeling *Braf*-induced thyroid cancer development and drug screening using pluripotent stem cell-derived organoids

Hélène Lasolle [1], Andrea Schiavo [1], Adrien Tourneur[1], Pierre Gilotay [1], Bárbara de Faria da Fonseca [1], Lucieli Ceolin [1, 6], Olivier Monestier [1], Benilda Aganahi [1], Laura Chomette [1], Marina Kisys Polisel [1], Lieven Haenabalcke [2], Tim Pieters [2, 3], Steven Goossens [2, 4], Jody Haigh [2, 5], Vincent Detours [1], Ana Luiza Silva Maia [6], Sabine Costagliola [1] and Mírian Romitti [1*]

[1] Institut de Recherche Interdisciplinaire en Biologie Humaine et Moléculaire (IRIBHM), Université Libre de Bruxelles (ULB), Brussels, Belgium

[2] VIB, Flanders Institute for Biotechnology, Ghent University, Ghent, Belgium

[3] Department of Biomolecular Medicine, Faculty of Medicine and Health Sciences, Ghent University, Ghent, Belgium

[4] Department of Diagnostic Sciences, Faculty of Medicine and Health Sciences, Ghent University, Ghent, Belgium

[5] CancerCare Manitoba Research Institute, Department of Pharmacology and Therapeutics, Rady Faculty of Health Sciences, University of Manitoba, Winnipeg, Manitoba, Canada

[6] Thyroid Section, Endocrine Division, Hospital de Clínicas de Porto Alegre (HCPA), Universidade Federal do Rio Grande do Sul (UFRGS), Porto Alegre, Brazil

* Corresponding author: mirian.romitti@ulb.be

Abstract

Thyroid cancer is the most common endocrine malignancy and several genetic events have been described to promote the development of thyroid carcinogenesis. Besides the effects of specific mutations on thyroid cancer development, the molecular mechanisms controlling tumorigenesis, tumor behavior, and drug resistance are still largely unknown. Cancer organoids have been proposed as a powerful tool to study aspects related to tumor development and progression and appear promising to test individual response to therapies. Here, using mESC-derived thyroid organoids, we developed a Braf^{V637E}-inducible model able of recapitulating the features of papillary thyroid cancer in vitro. Overexpression of Braf^{V637E} rapidly leads to MAPK activation, cell dedifferentiation, and disruption of follicular organization. Braf^{V637E}-expressing organoids show a transcriptomic signature for p53, focal adhesion, ECM-receptor interactions, EMT, and inflammatory signaling pathways. Finally, PTC-like thyroid organoids were used for drug screening assays. The combination of MAPK and PI3K inhibitors reversed *Braf* oncogene-promoted cell dedifferentiation while restoring thyroid follicle organization and function *in vitro*. Our results demonstrate that pluripotent stem cells-derived thyroid cancer organoids can mimic tumor development and features while providing an efficient tool for testing novel targeted therapies.

Introduction

Pluripotent Stem Cells (PSCs) emerged as a model to dissect and recapitulate the molecular events and gene networks that regulate cell fate determination, cell differentiation and organogenesis. Guided differentiation of PSCs into 3D organized tissue, by inducible overexpression of specific transcription or growth factors and inhibitors allows derivation of *in vitro* organoids and the understanding of mechanisms

51 regulating cell differentiation and tissue formation[1]. Due to their remarkable self-
52 organizing structures and functional properties, organoids technology became a powerful
53 tool to model organ development and disease 'in a dish' [2,3].

54 In the last decade, the use of organoids for cancer research emerged and opened
55 new possibilities to better understand tumor behavior. Initially, colon, prostate,
56 pancreatic, ovarian, lung and thyroid cancer derived organoids have been efficiently
57 generated which resemble phenotypically and genetically the tumour of origin[4–13].
58 Currently, a large set of healthy and tumour matching organoids has been generated and
59 available through biobanks. These patient-derived organoids are particularly interesting
60 to test individual response to therapies[8,13,14].

61 Recently, studies have reported the generation of cancer models arising from
62 healthy (adult stem cells or aSCs and PSCs) organoids by controlling oncogene
63 expression[15–17]. By using gene expression manipulation tools, such as shRNA and
64 CRISPR-Cas9, murine stomach cancer ($Cdh1^{-/-}$; $Tp53^{-/-}$)[18], murine and human colon
65 cancer (APC, TP53, KRAS and Smad4 mutations)[15,16,19], human pancreatic cancer
66 (KRAS and/or TP53 mutations)[4,20] and human lung adenocarcinoma organoids (HER2
67 overexpression) could be efficiently generated[17]. Compared to patient-derived organoids,
68 healthy stem cells-derived cancer organoids are suitable to address additional questions
69 such as precise effects of oncogenes and early events driving tumorigenesis; the role of
70 cancer stem cells on tumor induction, genomic stability, the effect of treatments at
71 different stages of carcinogenesis and screening for new therapeutical tools[21]. Besides,
72 they allow multiple reproductible experiments free from inter-individual variability.

73 Thyroid cancer is the most frequent endocrine malignancy and several genetic
74 events have been described driving thyroid carcinogenesis. Papillary thyroid carcinoma
75 (PTC) is the most common malignant thyroid tumor[22] and an aberrant activation of

76 MAPK pathway is a hallmark[23]. The BRAF^{V600E} mutation is the most frequent genetic
77 event, accounting for around 50% of PTCs[24–26] and results is an oncogenic protein with
78 markedly elevated kinase activity that constitutively induces the MAPK pathway, mainly
79 through MEK/ERK signaling transduction[27–29].

80 BRAF-mutated thyroid tumors are often less differentiated, mainly due to the
81 lower expression levels of thyroid functional genes *NIS, TSHR, TG* or *TPO* leading to a
82 low Thyroid Differentiation Score (TDS)[30]. This dedifferentiated state is associated with
83 a worse clinical condition and with higher rate of radioactive iodine (RAI) refractory
84 tumors[31,32]. However, its impact on prognosis is still uncertain, as BRAF^{V600E} alone has
85 not been proved to be an independent prognostic factor[33,34]. On the other hand, *BRAF* and
86 *TERT* promoter mutated tumors have been associated with higher specific mortality[35].
87 Also, studies have shown a small proportion (around 20%) of BRAF^{V600E} mutated tumors
88 presenting a higher level of differentiation which is associated to a less aggressive
89 behavior and a preserved RAI uptake ability[30,36]. This suggests a possible cell
90 heterogeneity among the BRAF^{V600E} mutated tumors.

91 Some years ago, our group showed the generation of functional 3D thyroid tissue
92 derived from mouse embryonic stem cells (mESC)[37] and recently human thyroid
93 organoids were generated using the same approach[38]. The differentiation protocol relies
94 on transient induction of *Nkx2.1* and *Pax8* thyroid transcription factors allowing an
95 efficient generation of thyroid follicular cells which organized into three-dimensional
96 follicular structures capable of thyroid hormone production *in vitro* and *in vivo*. This
97 model and further developed thyroid organoids from mouse and human healthy
98 PSCs/aSC[39–49] open new perspectives to explore thyroid development processes as well
99 as to model thyroid diseases, including thyroid cancer.

100 So far, efficient, fast and cost-effective tools are lacking to functionally characterize a

101 large set of candidate genes in the context of thyroid carcinogenesis. Thyroid cancer
102 organoids/spheroids models have been recently described which are based in patient
103 tumor-derived models[50–54]. Patient-derived organoid might be used to study patient-
104 specific tumor behavior and the treatment response in a case-to-case basis; however, it is
105 patient-to-patient dependent with high heterogeneity and low reproducibility; limited by
106 the accessibility to samples; and since it is derived from an already stablished tumor, it is
107 not suitable to study mechanisms related to cancer development and drugs resistance
108 acquisition. Saito et al. described a mouse model of poorly differentiated thyroid
109 carcinoma, obtained after transplantation of thyroid organoids derived from Tp53
110 knockout mice with NRAS activating mutation overexpression[12] . Recently, Veschi *et al.*
111 [55] generated of PTC and FTC organoids models, by inducing BRAF, NRAS and TP53
112 mutations in thyroid progenitors derived from hESC. After transplantation, the tumors
113 generated resemble Papillary and Follicular tumors and transcriptomics analysis
114 suggested a role of Kisspeptin receptor (KISS1R) in cooperation with Tissue Inhibitor of
115 Metalloproteinase 1 (TIMP1)/Matrix metallopeptidase 9 (MMP9)/Cluster of
116 differentiation 44 (CD44), on tumor development and progression[55].
117 Here, we aim to develop an *in vitro* PTC organoid model to screen for targets and
118 drugs, by taking advantage of our model of thyroid generation, by includible expression
119 of Braf^{V637E} mutation in mouse ESC-derived functional thyroid follicles.
120
121 **Methods**
122
123 *Cell culture and mESC_Braf^{V637E} line generation*

124 The previously genetically modified G4 RosaLuc mouse embryonic stem cell line
125 (mESC)[56] was initially cultured on gamma-irradiated mouse embryonic fibroblasts

126 (MEFs) feeder using mouse stem cell medium[37,57] and incubated at 37 °C, 5 % CO^2 and
127 >95 % humidity. To insert the target sequences into the modified Rosa26 locus of G4
128 RosaLuc mESCs, around $1x10^5$ cells were transfected using the Flpe expressing vector[56]
129 and the target vector containing the rtTA-TRE induction system, thyroid transcription
130 factors, Nkx2-1 and Pax8 and bTg-NES-$Braf^{V637E}$-ERT^2 sequences (Figure S1A)
131 following the lipofectamine 3000 protocol (Thermo Scientific). The $Braf^{V637E}$ mutation
132 here used for mouse cells is equivalent to the human $BRAF^{V600E}$ mutation[58]. G418 (300
133 µg/ml) was applied 48 h after transfection typically for 10 days and individual clones
134 were picked and further expanded. Clones were screened for by immunofluorescence for
135 Nkx2-1 and Pax8 expression induction after 3 days incubation with 1 µg/ml Doxycyclin
136 (Dox) (Figure S1B). Positive clones were then characterized according to pluripotency
137 maintenance (Figure S1C), levels of *Nkx2-1* and *Pax8* expression, and efficiency of
138 thyroid differentiation. In addition, we generated a mESC control line where the
139 sequences of NES-$BRAF^{V637E}$-ERT^2 were replaced by eGFP sequence, resulting in the
140 TRE-Nkx2-1-Pax8_bTg-eGFP line (Figure S1D). The mESC control line generation,
141 selection and characterization were performed as described above (Figures S1E and F).

142 *Thyroid differentiation protocol*

143 G4 RosaLuc TRE-Nkx2-1-Pax8_bTg-NES-$Braf^{V637E}$-ERT^2 and TRE-Nkx2-1-
144 Pax8_bTg-eGFP cells were cultured and differentiated as described previously by
145 Antonica *et al* (2012)[37] with few modifications. Briefly, embryoid bodies (EBs),
146 generated by hanging drops were collected after 4 days and embedded in growth factor
147 reduced Matrigel (GFR MTG; BD Biosciences); 50µl MTG drops (containing around 20
148 EBs) were plated into 12-wells plates. EBs were differentiated using a differentiation
149 medium initially supplemented with 1µg/ml of Doxycycline (Sigma) for 5 days, followed
150 by 2 weeks of maturation induction by using 0.3 nmol of 8-Br-cAMP (BioLog) or 1mU

151 ml^{-1} of thyrotropin (hrTSH; Genzyme). Thyroid differentiation and functionality were
152 evaluated by transcriptomics (RT-PCR and bulk RNA sequencing), immunofluorescence
153 and iodide organification.
154
155 *$Braf^{V637E}$ induction and drug screening*
156 After thyroid full maturation (Day 25), MTG drops were washed twice with Hanks's
157 balanced salt solution (HBSS, containing calcium and magnesium; Invitrogen) and
158 incubated in a HBSS solution (1 ml per well) containing 10 U/ml of dispase II (Roche)
159 and 125 U/ml of collagenase type IV (Sigma) for 30 min at 37°C. Then the enzymes were
160 inactivated by adding 10% FBS and cells were centrifuged at 500g for 3 min. Cells were
161 rinsed twice with HBSS and the follicles population was enriched by filtering using 30
162 μm (single cell removal) and 100 μm reverse strainer (Pluriselect). Finally, enriched
163 structures were re-embedded in GFR MTG (50μl) and plated into 12-well plates. Twenty-
164 for hours later, cells were incubated with 1 μM of 4-Hydroxytamoxifen (4OHT) (Sigma)
165 and 8-Br-cAMP or hrTSH for 24h, 48h or 7 days to promote $Braf^{V637E}$-induced
166 phosphorylation of MAPK pathway[58].
167 In addition, Braf-induced thyroid organoids (previously treated for 4 days with 4OHT)
168 were cultured with distinct compounds, previously suggested to regulate Nis re-
169 expression and inhibit *Braf* oncogenic effects[59,60]. Among the screened drugs, several
170 cell processes were targeted by the following compounds: PD0325901 (MEK inhibitor;
171 250nM; Stem Cell), LY204002 (PI3K inhibitor; 5μM; Selleckchem), VPA (HDAC
172 inhibitor; 250μM; Sigma), NAC (N-acetyl cysteine, antioxidant compound; 2mM;
173 Sigma), 5-AZA-2' deocytidine (DNA methyltransferase (DMNT) inhibitor; 1μM;
174 Sigma) and RG108 (DMNT inhibitor; 10μM; Sigma).
175

176 *Flow cytometry - Proliferation analysis*

177 Control condition (4OHT-) and organoids treated with 4OHT for 6 days were treated with
178 BrdU (1mM) for 3 hours, collected and prepared for immunostaining as follows: Matrigel
179 drops (at least 5 samples per condition) were first digested with HBSS solution containing
180 10 U/ml dispase II and 125 U/ml collagenase type IV for 30-60 min at 37°C; then a single
181 cell suspension was obtained by dissociation with TripLE Express for 10-15 min
182 incubation at 37°C, the enzymes were inactivated by addition of differentiation medium.
183 After centrifugation, samples were rinsed with PBS and then the BrdU Flow Kit staining
184 protocol (BD) was used according to the manufacturer's instructions. In order to identify
185 the BrdU incorporated cells among the thyroid population, cells were also stained using
186 primary Nkx2-1 antibody (1:100) and anti-rabbit IgG Alexa fluor 647-conjugated
187 secondary antibody (1:300). Non-stained and only secondary-incubated cells were used
188 as negative control for gate strategy. LSR-Fortessa X-20 flow cytometer was used for
189 quantification and FACSDiva software used for the analysis. Data is presented as
190 percentage of positive cells.

191

192 *Immunofluorescence staining*

193 Organoids embedded in MTG were fixed in 4% paraformaldehyde (PFA; Sigma) for 1 h
194 at room temperature (RT) and washed three times in PBS. Blocking was performed using
195 a solution of PBS containing 3% bovine serum albumin (BSA; Sigma), 5% horse serum
196 (Invitrogen) and 0.3% Triton X-100 (Sigma) for 30 min at RT. The primary and
197 secondary antibodies were diluted in a solution of PBS containing 3% BSA, 1% horse
198 serum and 0.1% Triton X-100. Primary antibodies were incubated overnight at 4°C
199 followed by incubation with secondary antibodies and Hoechst for 2 h at RT. Slides were
200 mounted with Glycergel (Dako).

201 For paraffin embedding, organoids were fixed overnight at 4°C in 4% PFA and kept in
202 70% ethanol at 4°C before embedding. Samples were then embedded in paraffin,
203 sectioned (5 μm), mounted on glass slides, deparaffinized, and rehydrated. For
204 immunostaining, antigen retrieval was performed by incubating the sections for 10 min
205 in the microwave (850 W) in Sodium Citrate Buffer (10 mM Sodium Citrate, 0.05%
206 Tween 20, pH 6.0). After cooling, the sections were rinsed with PBS and blocked with
207 1% BSA and 10% horse serum PBS solution for 1 h at RT. Primary antibodies were
208 diluted (as described above) in the blocking solution and incubated overnight at 4°C. The
209 sections were rinsed three times in PBS and incubated with Hoechst and secondary
210 antibodies diluted in blocking solution for 1 h at room temperature. Slides were mounted
211 with Glycergel (Dako). Imaging was performed using a Zeiss LSM510 META confocal
212 microscope and a Leica DMI6000 microscope with DFC365FX camera. The antibodies
213 information is listed in the supplementary Table 1.
214
215 *Western blot*
216 Organoids were initially isolated (collagenase IV/dispase II solution, described above)
217 from at least 6 distinct wells and pooled together for proteins extraction using RIPA
218 buffer. The protein concentration was determined according to Pierce 660 nm protein
219 assay reagent protocol (Thermo Scientific). Briefly, 30–50 μg protein of each sample was
220 fractionated by 10% SDS–PAGE and blotted onto an Immobilon PVDF membrane
221 (Millipore). Blocking of non-specific binding sites were blocked by incubation with 5%
222 BSA in Tris-buffered saline (TBS) 0.1% Tween-20 for 1 h. Thereafter, the membrane
223 was incubated overnight at 4 °C with primary antibodies against p-ERK and β-Actin in
224 blocking solution. Next, the membrane was incubated with horseradish peroxidase-
225 conjugated anti-rabbit or anti-mouse antibody in blocking solution, for 60 min at RT. The

226 antigen–antibody complexes were visualized using an enhanced chemiluminescence
227 system (GE Healthcare) and captured by Azure 500 system (Azure Biosystems).
228
229 *Iodide organification assay*
230 Thyroid organoids treated with cAMP, cAMP+4OHT, cAMP+4OHT+PD+LY and
231 cAMP+4OHT+PD+LY+VPA were tested for the ability of iodide uptake and
232 organification as previously described[37,57]. Briefly, cells were washed with HBSS and
233 incubated with 1 ml per well of an organification medium containing 1,000,000 c.p.m.
234 per ml ^{125}I (PerkinElmer) and 100 nM sodium iodide (NaI, Sigma) in HBSS for 2 h at 37
235 °C. After, the reaction was stopped by addition of methimazole (MMI; 4 mM, Sigma).
236 After two cold PBS washes, cells were detached using trypsin/EDTA (Invitrogen). For
237 iodide uptake quantification, cells were collected, and radioactivity was measured using
238 a c-counter. Subsequently, proteins were precipitated by adding 1 mg of gamma-globulins
239 (Sigma) and 20% TCA followed by centrifugation at 2,000 r.p.m. for 10 min, at 4°C and
240 the radioactivity of protein-bound ^{125}I (PBI) was measured. Iodide organification was
241 calculated as an iodide uptake/PBI ratio and the values expressed as a percentage. Cells
242 were also treated with 1 mM sodium perchlorate (Nis inhibitor; NaClO4, Sigma-Aldrich)
243 and 2 mM MMI (Tpo inhibitor; Sigma-Aldrich) as iodide uptake and protein-binding
244 controls, respectively. The experiments were performed in triplicates for each condition.
245
246 *Gene expression analysis*
247 Real time PCR (RT-qPCR) was performed on cDNA from thyroid organoids from at least
248 three independent experiments. Total RNA was extracted from thyroid organoids by
249 addition of lysis RLT Lysis buffer (Qiagen) + 1% 2-mercaptoethanol directly on the MTG
250 drop containing the organoids. RNA was isolated using RNeasy micro kit (Qiagen)

251 according to the manufacturer's instructions. cDNA was generated by reverse
252 transcription using Superscript II kit (Invitrogen). qPCR was performed on cDNA in
253 triplicates using Takyon™ No ROX SYBR 2X MasterMix blue dTTP (Eurogentec) and
254 CFX Connect Real-Time System (Biorad). Results are presented as linearized values
255 normalized to the housekeeping gene, β2-microglobulin and the indicated reference value
256 (2-DDCt). Primers sequences are described in the supplementary table 2.

257 *Bulk RNA sequencing and analysis*

258 Bulk RNA-seq was performed at day 31, using the cAMP, cAMP+4OHT (5 days) and
259 cAMP+4OHT+PD+LY (3 days) conditions (see protocol, Figure 5A). RNA extraction
260 was performed as previously described (section "*Gene expression analysis"*) and
261 experiments were performed in duplicates. At least 3 distinct wells were pooled together
262 for each condition. RNA quality and concentration were evaluated using Bioanalyser
263 2100 (Agilent) and RNA 6000 Nano Kit (Agilent). RNA integrity was preserved, and no
264 genomic DNA contamination was detected. Indexed cDNA libraries were obtained using
265 the TruSeq Stranded mRNA Sample Prep kit (Illumina) using a S2 flow cell and
266 sequences were produced using a 200 cycles reagent kit. The resulting high-quality
267 indexed cDNA libraries were quantified with the Quant-iT PicoGreen kit (Life Sciences)
268 and Infinite F200 Proplate reader (Tecan); DNA fragment size distribution was examined
269 with the 2100 Bioanalyzer (Agilent) using the DNA 1000 kit (Agilent). Multiplexed
270 libraries (10ρM) were loaded onto flow cells and sequenced on the HiSeq 1500 system
271 (Illumina) in high-output mode using the HiSeq Cluster Kit v4 (Illumina). The sequenced
272 data were uploaded on the galaxy web platform version 22.05.1 and the public sever
273 https://usegalaxy.eu was used for mapping and counting analysis. Approximately 10
274 million paired-end reads were obtained per sample. After the removal of low-quality
275 bases and Illumina adapter sequences using Trimmomatic software[61], paired-end reads

276 were mapped against the mouse reference genome mm10 (GRCm38) using HISAT2
277 sofware[62], allowing soft clipping. Raw read counts were obtained using HTseq count
278 software with unstranded option[63]. Low expressed genes were filtered using EdgeR
279 package in R software (https://www.r-project.org). Then, differential expression analysis
280 was performed using DESeq2 package[64]. Fold change and adjusted p-value thresholds of
281 2 and 0.05 respectively were used to select differentially expressed genes (DEG). Gene
282 ontology and pathways enrichment analysis in up and down differentially expressed
283 genes lists was realized using EnrichR (https://maayanlab.cloud/Enrichr/). Transformed
284 counts corresponding to log2 (normalized counts +4) using DESeq2 package were used
285 for further analysis and heatmap visualization. Thyroid differentiation score (TDS),
286 Enhanced Thyroid differentiation score (eTDS) and ERK activation score were calculated
287 as previously described[65]. The list of the genes used for the score's calculation is provided
288 in the supplementary table 3.
289
290 *Data availability*
291 The data that support this study are available from the corresponding author upon request.
292 Bulk RNA-seq data have been deposited in the NCBI Gene Expression Omnibus under
293 accession number GSE228281.
294
295 *Statistical analysis*
296 All statistics analysis were performed using GraphPad Prism 9. Comparison between two
297 groups and its statistical significance was tested using the unpaired *t* test or nonparametric
298 Mann-Whitney U test, while comparison between multiple groups was performed using
299 one-way ANOVA or nonparametric Kruskal-Wallis test. Data are displayed as mean ±
300 SD or median (IQR). Differences were considered significant at $p<0.05$ and presented as

301 follows: *p < 0.05, **p < 0.01, ***p < 0.001, ****p < 0.0001. All the data presented are
302 from at least three independent experiments.
303
304 **Results**
305 *mESC_BRAF^{V637E} cell line generation and characterization*
306 We combined the previously described mESC transient induction thyroid differentiation
307 strategy (Antonica, 2012) with a Braf^{V637E}-ERT^2 inducible model (Ortiz, 2013) to
308 generate a double-inducible recombinant mESC_BRAF^{V637E} cell line. The resulting
309 mESC_Nkx2-1/Pax8_bTg_Braf^{V637E}_ERT^2 clones were initially selected and
310 characterized by the response to doxycycline (Dox) treatment, confirmed by the
311 overexpression of Nkx2-1 and Pax8; and ability to spontaneously differentiate into cells
312 from the three germ-layers (Figures S1A, B and C, respectively). In addition, a control
313 mESC line was generated in which Braf^{V637E}_ERT^2 system was replaced by eGFP
314 sequence. Similarly, the control line showed a proper response to Dox induction and
315 maintained the pluripotency capacity (Figures S1D, E and F, respectively).
316
317 *Thyroid differentiation protocol*
318 The capability of the new cell line to generate thyroid follicles and express the Braf^{V637E}
319 oncogene was demonstrated following the mESC thyroid differentiation protocol
320 (Antonica, 2012; Antonica, 2017; Romitti, 2021). Since we used a newly modified mESC
321 line, the steps of the differentiation protocol were tested and adapted accordingly (Figure
322 1A). Here, using the mESC_Nkx2-1/Pax8_bTg_Braf^{V637E} line, we observed that Dox
323 stimulation for 5 days lead to higher levels of exogenous and endogenous *Nkx2-1*, *Pax8*
324 and *Tg* mRNA (day 9; Figure S2E) compared to 3 or 4 days of treatment (Figure S2A-
325 D). Similar results were obtained using the control mESC line (Figure S2A-D). Next, two

326 weeks of treatment with cAMP (from day 9 to 23) markedly induced the expression levels
327 of *Nkx2-1, Pax8, Tg, TshR, Nis* and *Tpo* when compared to the control (-Dox -cAMP)
328 (Figure 1B). Accordingly, immunofluorescence staining showed follicular organized
329 Nkx2-1 and Tg expressing cells (Figure 1C) in which the functionality is demonstrated
330 by intraluminal iodinate-Tg (Tg-I) accumulation (Figure 1D). Since our protocol also
331 generate other cell types than thyroid[57], a follicle enrichment step was added to the
332 protocol to enrich the follicular structures and induce Braf-oncogene in an purer
333 population. This protocol led to an increase of thyroid markers levels (Figure 1E) when
334 compared to non-enriched control condition, while the follicular structure and
335 functionality were preserved as demonstrated by Nkx2-1, Nis and Tg-I staining (Figure
336 1F-G). Notably, after re-embedding in Matrigel (MTG) follicles could be maintained in
337 culture for at least 28 additional days without major histological changes (data not
338 shown).
339
340 *Braf^{V637E} induction on thyroid organoids leads to PTC-like phenotype*
341 To ensure that Braf^{V637E} oncogene is expressed specifically among follicular thyroid cells,
342 we used the bovine Tg (bTg) as promoter controlling Braf^{V637E}_ERT^{2} expression.
343 Effectively, exogenous *Braf^{V637E}* mRNA expression was rapidly induced after Dox
344 treatment (Day 9; Figure S2E), maintaining the expression levels stable over time (Figure
345 1B and Figure S3A), while *Tg* mRNA expression increased following the differentiation
346 program (Figure S3A). Even if *Braf^{V637E}* expression is driven by bTg promoter, the Braf-
347 mutated protein is not active/phosphorylated since it is maintained in the nucleus in an
348 inactive complex with HSP90. The addition of 4OHT induces nuclear translocation of the
349 Braf mutant to the cytoplasm (NES signal) then driving MAPK activation (Ortiz, 2013)
350 (Figure 2A). Indeed, 24 hours after 4OHT addition we observed an increase in ERK

351 phosphorylation (pERK) compared to the control condition (cAMP), which was
352 maintained after 7 days of continuous 4OHT treatment (Figure 2B). To assess Braf-
353 induced cell proliferation, flow cytometry analysis performed after 6 days of 4OHT
354 treatment demonstrated increased proportion of Nkx2-1/BrdU+ cells among the
355 $Braf^{V637E}$-expressing condition (4OHT) compared to the control (cAMP) (Figure 2C).

356 One of the hallmarks of thyroid cancer development is the downregulation of
357 thyroid differentiation markers (Mitsutake, 2005; Chakravarty, 2011). Indeed, the
358 activation of $Braf^{V637E}$ rapidly led to a progressive time-dependent decrease of *Tpo*, *TSHR*
359 and *Tg* mRNA expression (Figures 2D-F and S3B), detected as early as 6 hours after
360 4OHT addition (Figure 2D). Notably, more significant downregulation was observed
361 after 48 hours and maintained for at least 7 days (Figures 2E-F, respectively). As
362 described among PTCs, in our model the expression of thyroid transcription factors *Pax8*
363 and *Nkx2-1* was also globally maintained. Conversely, *Lgals3 (Galectin 3)* expression,
364 which has been suggested as a marker for thyroid malignancies and more specifically for
365 PTC[66], was significantly increased in both time points (Figures 2E-F). Also, increase in
366 Fibronectin 1 (*Fn1*) expression, which has been associated with aggressive thyroid
367 cancer[67,68], was observed after 7 days of $Braf^{V637E}$ induction, suggesting a more advanced
368 dedifferentiated cell state in our organoid model (Figure 2F). Similar results were
369 obtained when cells were differentiated using hrTSH instead of cAMP and $Braf^{V637E}$ was
370 induced in such conditioned media, indicating that the phenotype is not dependent of TSH
371 signaling (data not shown).

372 Histological analysis performed after 48 hours of continuous activation of
373 $Braf^{V637E}$ by 4OHT, demonstrated disruption of the follicular organization in non-
374 enriched thyroid organoids compared to control condition (cAMP) (Figure 3A). Nkx2-1
375 and Tg staining revealed that $Braf^{V637E}$ oncogene strongly disturbs thyroid follicles

376 forming elongated and unorganized structures. In addition, heterogenous expression of
377 Tg was observed among the Nkx2-1 cells. Further analysis, performed in follicle enriched
378 population, confirmed the effect of *Braf* oncogene in promoting cell dedifferentiation and
379 loss of follicle organization. Tg levels were overall reduced and heterogeneous among
380 the unorganized Nkx2-1+ cells (Figure 3B). Interestingly, the cell disorganization caused
381 by Braf oncogene might pass by an initial expansion of the follicular size with infiltration
382 of Nkx2-1 cells inside of the lumen compartment, which also presents a heterogeneous
383 distribution of Tg (Figure S3C), since this feature was observed among some "follicular-
384 like" remaining structures after 48 h of 4OHT treatment. Reassuringly, staining for E-
385 Cadherin (epithelial) and Zo-1 (intra-luminal) adhesion markers showed that $Braf^{V637E}$-
386 expressing cells (Nkx2-1) are not able to preserve polarization and consequently lumen
387 space is not well defined in most of the structures (Figures 3C-D, respectively).
388 Consequently, the functionality of those cells was impaired and Tg-I accumulation was
389 significantly reduced compared to the control condition (Figure 3E). Of note, despite the
390 strong effect of $Braf^{V637E}$ oncogene on thyroid follicles disruption, we observed that few
391 follicles still preserved certain degree of organization (Figure S3D) after 48 h of 4OHT
392 treatment. As expected, after 7 days of $Braf^{V637E}$ continuous stimulation, a higher level of
393 cell dedifferentiation and lack of organization could be detected, with a lower proportion
394 of the Nkx2-1 cells expressing Tg compared to control (Figure 3F) and to the previous
395 time point (48 h; Figure 3A). The above-described experiments were also performed
396 using the control TRE-Nkx2-1-Pax8_bTg-eGFP cell line. The addition of 4OHT to
397 mature follicles (from day 27 to day 36) did not impair thyroid differentiation markers
398 gene expression and follicles organization (Figures S3E-F). On the other hand, slightly
399 induction of *Nkx2.1, Pax8, Tg, TshR, Tpo and Nis* levels was observed under cAMP co-
400 treatment with 4OHT (Figure S3E).

401 *Effect of transient Braf^{V637E}-induction on cell differentiation*

402 Since in our system for Braf^{V637E} activation is dependent of continuous treatment with
403 4OHT we transiently treated the cells with 4OHT for 2 days followed by 5 days culture
404 in 4OHT-free medium (cAMP) in order to explore if the oncogenic effect is maintained
405 when the protein is not active. Surprisingly, we did not observe recovery of *Nkx2-1,*
406 *TSHR, Tg* or *Tpo* gene expression levels (Figures 4A-E) after 4OHT removal. However,
407 *Pax8* and *Slc5a5/Nis* expression were partially recovered (Figure 4F), confirming the
408 specific inhibitory effect of *Braf* oncogene on *Slc5a5/Nis* expression. These findings
409 indicate that *Nis* regulation mechanisms are maintained in our system and suggests it as
410 tool for Nis-reactivation studies.

411

412 *Screening for Nis re-expression using signaling pathways inhibitors*

413 Studies in mouse models and humans have demonstrated that tumors carrying *Braf*
414 mutations show reduced expression of *Nis* and consequently higher rate of radioiodine
415 (RAI) refractoriness[28,31,65]. Here, taking advantage of our PTC organoid model we aim to
416 explore new strategies to reactivate *Nis* expression in Braf^{V637E}-expressing cells by
417 screening distinct categories of inhibitors previously described to be involved on *Nis*
418 regulation [59,60]. PD0325901 (MEK inhibitor), LY204002 (PI3K inhibitor), VPA (HDAC
419 inhibitor), NAC (N-acetyl cysteine, antioxidant compound), 5-AZA-2' deocytidine and
420 RG108 (DMNT inhibitors) were tested isolated and/or in combination for 3 days (in
421 addition to cAMP+4OHT) using Braf^{V637E}-expressing organoids (after 4 days of
422 cAMP+4OHT treatment; Figure 5A). Initially, we observed that VPA alone was the only
423 treatment able to completely restore *Nis* expression levels (Figure 5B-C and S4A).
424 However, when combined, PD0325901 and LY204002 inhibitors; PD0325901,
425 LY204002 and VPA; and PD0325901 and Nac resulted in great increase of *Nis* mRNA

426 (Figure 5B-C and S4A). IF staining shows Nis protein re-expression among Braf^{V637E}-
427 induced cells treated with VPA alone, but localization was not restricted to the membrane.
428 In contrast, when cells were treated with MEK of PI3K inhibitors, associated or not with
429 VPA, we observed Nis protein at the apical membrane and, surprisingly, the follicular
430 structure also seems to be restored (Figure 5C).
431
432 *MAPK and PI3K signaling inhibition cause Braf-induced cells redifferentiation and*
433 *function recovery*
434 Since we observed that HDAC, MEK and PI3K inhibition seems to favor follicle
435 reorganization, we evaluated if such treatments also induce cell redifferentiation and
436 function recovery. Initially we analyzed the gene expression levels of thyroid
437 differentiation markers strongly affected by Braf-induction. The effects of isolated and
438 combined drugs on *Tg, TSHR, Tpo, Nkx2-1* and *Duox* genes appear to be variable and
439 pathway dependent (Figure S4B-F). As with *Slc5a5/Nis*, MEK and PI3K inhibition in
440 combination with or without VPA resulted in complete recovery of *Tg*, *TSHR* and *Tpo*
441 mRNA levels (Figures 6A-C), indicating cell redifferentiation. While *TSHR* levels can be
442 restored by treatment with isolated inhibitors (Figure 6B), *Tpo* expression appears to be
443 dependent on PI3K signaling (Figure 6C). On the other hand, *Tg* mRNA expression is
444 recovered only when the inhibitors are used in combination (Figure 6A). Indeed,
445 immunostaining showed that isolated inhibitors could not restore Tg levels. Nevertheless,
446 a higher proportion of Tg-expressing cells was observed with the MEK inhibitor,
447 PD0325901 (Figure S4G). Conversely, combined MEK and PI3K inhibitors restored Tg
448 protein levels and generated a similar proportion of expressing follicles as under the
449 cAMP condition (Figures 6D-E).

450 Considering that inhibition of MEK and PI3K pathways (+/-VPA) promote recovery of
451 thyroid redifferentiation and follicular organization, we tested the functionality of
452 reorganized follicles. Remarkably, we observed an accumulation of Tg-I in the lumen of
453 follicles treated with the combinations of inhibitors (Figure 6F). Organification assay
454 confirmed that the co-treatment, restored iodide uptake and ^{125}I binding to proteins
455 resulting in organification levels comparable to the control (Figure 6G-I).
456
457 *Transcriptomic characterization of PTC model and drug screening tests*
458 Transcriptomic analysis of cAMP, cAMP+4OHT and cAMP+4OHT+PD+LY (Figure
459 5A) confirmed downregulation of thyroid genes under Braf-oncogene stimulation (4OHT
460 condition) whereas global recovery of expression was observed under inhibitors
461 treatment (Figure 7A). Accordingly, thyroid differentiation scores (TDS and enhanced
462 (e)TDS) were decreased under Braf^{V637E} induction while they recovered in the presence
463 of inhibitors (Figure 7B). Conversely, ERK activation score was higher in the Braf^{V637E}
464 samples and decreased sharply under inhibitor conditions (Figure 7C). Considering that
465 bulk RNAseq was performed using the follicle-enriched population, the presence of non-
466 thyroid cells is reduced compared with the original whole organoids, but still present.
467 This may explain the modest increase in ERK score among Braf-activated cells while the
468 apparent decrease under the condition with inhibitors, reflects the effect of the treatment
469 on each cell type.
470 Differential expression analysis identified 321 Differential Expressed Genes (DEGs; 156
471 upregulated and 165 downregulated genes) in 4OHT condition compared to cAMP; and
472 853 DEGs in inhibitors compared to 4OHT (287 upregulated and 566 downregulated
473 genes). Gene enrichment classification analysis of DEGs results are presented in Figures
474 7D-G. Briefly, among the upregulated genes in Braf-induced compared to control we

475 observed gene signature for the hyperactivation of PI3K-AKT-mTOR, TNF and
476 cytokines signaling and promotion of Epithelial Mesenchymal transition (EMT) (Figure
477 7D). While genes associated to thyroid hormone production, TGF-beta, Wnt/Beta-
478 Catenin pathway and regulation of angiogenesis were down-regulated (Figure 7E).
479 Conversely, inhibitor's treatment compared to 4OHT condition, evidenced upregulation
480 of genes associated to thyroid hormone production, cell-cell contact, extra-cellular matrix
481 organization and angiogenesis processes (Figure 7F); while PI3K, MAPK, TNF,
482 cytokines signaling, ECM-receptor interactions and EMT-related genes were
483 downregulated (Figure 7G).
484

485 **Discussion**

486 Here, we described a Braf-oncogene derived thyroid cancer organoid model
487 recapitulating patient tumor features. *In vitro* thyroid cancer models that recapitulate
488 tumor development and behavior can facilitate the identification of early tumor drivers
489 and enable the screening of a large number of new drugs for the treatment of thyroid
490 cancer without the need to use too many animal models. By combining our previous
491 thyroid organoid model derived from mESCs with an inducible system, the $Braf^{V637E}$
492 oncogene could be specifically induced in mature Tg-expressing cells to obtain a 3D *in*
493 *vitro* cancer model. Overexpression of $Braf^{V637E}$ rapidly led to MAPK activation with an
494 increase of pERK, cell dedifferentiation and disruption of follicular organization. Similar
495 effects have been described in genetically modified mouse models[28,69,70]. Furthermore,
496 the gene expression signature of our cancer organoids confirmed the findings found in
497 the PTC samples which also showed enrichment of genes associated to p53, focal
498 adhesion, ECM-receptor interactions, EMT and inflammatory pathways[71–73].

499 Activating mutations in the *BRAF* gene are found in approximately 7% of all
500 human solid tumors, being particularly common in PTCs, ATCs and melanomas. In
501 addition, they have been reported less frequently in colorectal cancers (CRCs), lung
502 cancers, pediatric low-grade gliomas (PLGGs), glioblastomas, breast cancers and serous
503 ovarian cancers[74–80]. In PTCs and melanomas, $BRAF^{V600E}$ mutation seems to be
504 associated with a higher degree of dedifferentiation and more aggressive histological
505 patterns, but its prognostic role is still debated as it was not found independently of
506 histological features[33,34]. Nevertheless, studies suggest that $BRAF^{V600E}$ might predict
507 response to tyrosine kinase inhibitors (TKIs) in melanoma and lung cancer[81,82].

508 Surgery remains as the first choice for thyroid cancer therapy. Recommended post
509 operative treatment includes TSH suppression and RAI ablation particularly as adjuvant
510 treatment for patients at high risk for tumor recurrence and to treat patients with
511 persistent/recurrent or metastatic disease[83]. The benefit of RAI has been demonstrated in
512 patients by reducing the risk of recurrence and disease-related mortality[84]. However,
513 approximately two thirds of metastatic DTC become radioiodine refractory (RR-DTC),
514 defined by the absence of iodine uptake or tumor progression despite uptake[85,86]. There
515 is no curative treatment for radioiodine refractory DTCs and the recommended first-line
516 systemic treatment when local therapies are not possible is targeted therapies using
517 mainly multitarget TKIs, such as Lenvatinib, which showed a progression free survival
518 of 18 months [65,87–89]. However, it leads to frequent resistance and adverse effects.

519 NIS, a basal membrane iodide transporter, plays a critical role in radioiodine
520 accumulation in DTC cells and its level is closely related to response to RAI (I^{131}) therapy.
521 Studies in mouse models and humans have shown that the presence of *BRAF* mutations
522 results in lower *Nis* levels and consequently a higher rate of RAI-refractory tumours[28,31].
523 Here, we confirmed that this regulation is preserved in our cancer organoids, as disruption

524 of *Braf* activation led to in recovery of *Nis* levels. As TKIs, retinoic acids (RA), histone
525 deacetylase inhibitors (HDAC), peroxisome proliferator-activated receptor-gamma
526 (PPARG) have been tested to promote redifferentiation and *NIS* re-expression of RR-
527 DTCs, to suggest RAI treatment after a short, targeted treatment[87,90–92]. This strategy
528 could lead to tumor response while limiting adverse effects and several clinical trials are
529 ongoing. However, re-expression of NIS is not sufficient to explain the response to
530 redifferentiation therapeutics and RAI treatment. Membrane trafficking and the cellular
531 machinery that concentrate and retain iodine must be preserved[93] in a follicular
532 organization. Our model is proving to be a potential tool for redifferentiation studies
533 because of its ability to test large sets and combinations of treatments and to assess
534 follicular reorganization and iodide organification capacity using a functional assay that
535 is likely to be more strongly associated with response to RAI treatment than *NIS* mRNA
536 levels. $Braf^{V637E}$-expressing cells treated with VPA, MAPK and PI3K inhibitors showed
537 re-expression of *Nis* and corresponding uptake of radioactive iodide. Interestingly, the
538 combination of inhibitors also promoted restoration of thyroid markers, follicular
539 organization, and iodide organification ability. Interestingly, an ongoing clinical trial is
540 testing the effect of BKM120, a PI3K inhibitor, in patients with progressive, metastatic,
541 refractory, follicular or poorly differentiated thyroid cancers (NCT01830504). However,
542 the association with MAPK inhibitors is still not evaluated in patients with thyroid cancer.
543 In *BRAF*-mutated tumors, studies have shown that the combination of TKIs
544 therapies appears to be more effective and circumvents primary and/or acquired
545 resistance to TKI therapy. Often, resistance is due to reactivation of the MAPK/ERK
546 pathway or activation of other signaling pathways such as PTEN, NF-1 or RAS. It may
547 also result from hyperactivation of tyrosine kinase receptors, such as PDFRβ, IGF-1R and
548 HGF, which lead to activation of the AKT/PI3K pathway[94]. Studies in patients with

549 advanced melanoma carrying a BRAF^{V600E} mutation have shown that the combination of
550 BRAF and MEK inhibitors resulted in a higher rate of complete/partial responses and
551 median progression-free survival compared with monotherapy groups[95–97]. Such
552 important results lead to the use of drug combinations as standard treatment for these
553 patients[98,99].

554 In summary, we have developed a Braf oncogene-expressing thyroid cancer in
555 vitro organoid model from mESCs that recapitulates transcriptomic and histological
556 features of PTCs at early and advanced stages. Moreover, we demonstrated that the
557 combination of MEK and PI3K inhibitors promotes *Nis* re-expression and cell re-
558 differentiation leading to restoration of follicular structures and thyroid functionality.
559 Considering the robustness of this *in vitro* model which allows controlled induction of
560 the major thyroid oncogene in a three-dimensional system, its efficiency and simplicity,
561 our model can be used to study mechanisms associated with thyroid cancer development
562 and progression, thyroid redifferentiation and drug screening.

563

564 **Limitations of the study**

565 Although this in vitro model generates cancer organoids that recapitulate features
566 observed *in vivo* and it can be used as a powerful tool for drug screening, further work is
567 needed to fully explore the mechanisms associated with to tumorigenesis and long-term
568 cancer behavior. In our system, because Braf^{V637E} mutation is driven by the bTg promoter,
569 it enables specificity of expression for thyroid cells. On the other hand, dedifferentiation
570 caused by the oncogenic process may lead to downregulation of Braf oncogene
571 expression. Although pERK activation is still higher after 7 days of 4OHT treatment
572 compared with the control, this limits the use of this model for long-term cultures and
573 studies. Another technical limitation of this model is the lack of a thyroid-specific reporter
574 that would allow tracking of Braf^{V637E}-induced morphologic changes on follicular

575 structures by live imaging and the purification of cells for transcriptome analysis, which
576 was performed here in a bulk of enriched thyroid cells, which may hide some findings.
577 In addition, we did not explore early events associated with Braf^{V637E}-induced
578 transformation of thyroid cells, which could provide new insights into the early effectors
579 of thyroid carcinogenesis.
580

581 **Acknowledgements and Funding**

582 The authors acknowledge the ULB flow cytometry platform (C. Dubois), the ULB
583 genomic core facility (F. Libert and A. Lefort), LiMIF platform for confocal microscopy
584 (J.-M. Vanderwinden). We acknowledge the funding agencies that supported this study.
585 The Belgian National Fund for Scientific Research (FNRS) (PDR T.0140.14; PDR
586 T.0230.18, CDR J.0068.22, Televie 7.4633.17/7.4526.19) and the Fonds
587 d'Encouragement à la Recherche de l'Université Libre de Bruxelles (FER-ULB). The
588 Belgian Fondation contre le cancer (F/2020/1402; V.D.). FNRS (Chargé de Recherche,
589 No.825745; M.R.). The cooperation program CAPES-WBI (S.C. and A.L.M). The
590 Brazilian National Council for Scientific and Technological Development (CNPq; M.R.
591 and A.L.M), the Coordination for the Improvement of Higher Education Personnel
592 (CAPES; M.R. and A.L.M), the Brazilian Society of Endocrinology and Metabolism
593 (SBEM; M.R. and A.L.M) and the Fundação de Amparo à Pesquisa do Estado do Rio
594 Grande do Sul (FAPERGS; A.L.M). S.C is Research Director at FNRS. M.R is researcher
595 at ULB.
596

597 **Author contributions**

598 H.L., S.C. and M.R. developed the project, designed the experiments and analyzed the
599 data. L.H., T.P., S.G. and J.H. generated the plasmids and the G4 Rosaluc mESC line.

600 M.R. and A.S. generated the G4 RosaLuc TRE-Nkx2-1-Pax8_bTg-NES-Braf^{V637E}-ERT^{2}
601 and TRE-Nkx2-1-Pax8_bTg-eGFP cell lines. H.L., M.R., B.F.F., A.S., O.M., L.C.,
602 M.K.P. B.A., L.C., performed the *in vitro* experiments and protocol set up. M.R. and P.G.
603 obtained confocal images. H.L., M.R. and A.T. performed bulk RNA-Sequencing and
604 analyzed the results. H.L. and A.T. performed the bioinformatics analysis. H.L. and M.R.
605 wrote the first draft and A.L.M. and S.C. edited the manuscript. S.C., M.R. and A.L.M.
606 acquired funding for the project. All authors contributed to the article and approved the
607 submitted version.
608

609 **Competing interests**

610 All authors declare no competing interests.
611

612 **Correspondence** and requests for materials should be addressed to Mírian Romitti.
613

614 **References**

615 1. Schutgens, F. & Clevers, H. Human Organoids: Tools for Understanding Biology
616 and Treating Diseases. *Annual Review of Pathology: Mechanisms of Disease* **15**,
617 211–234 (2020).
618 2. Clevers, H. Modeling Development and Disease with Organoids. *Cell* **165**, 1586–
619 1597 (2016).
620 3. Kim, J., Koo, B. K. & Knoblich, J. A. Human organoids: model systems for human
621 biology and medicine. *Nature Reviews Molecular Cell Biology* vol. 21 571–584
622 Preprint at https://doi.org/10.1038/s41580-020-0259-3 (2020).
623 4. Boj, S. F. *et al.* Organoid Models of Human and Mouse Ductal Pancreatic Cancer.
624 *Cell* **160**, 324–338 (2015).
625 5. Gao, D. *et al.* Organoid Cultures Derived from Patients with Advanced Prostate
626 Cancer. *Cell* **159**, 176–187 (2014).
627 6. Sato, T. *et al.* Long-term Expansion of Epithelial Organoids From Human Colon,
628 Adenoma, Adenocarcinoma, and Barrett's Epithelium. *Gastroenterology* **141**,
629 1762–1772 (2011).
630 7. van de Wetering, M. *et al.* Prospective Derivation of a Living Organoid Biobank
631 of Colorectal Cancer Patients. *Cell* **161**, 933–945 (2015).
632 8. Drost, J. & Clevers, H. Organoids in cancer research. *Nat Rev Cancer* **18**, 407–418
633 (2018).

634 9. Gleave, A. M., Ci, X., Lin, D. & Wang, Y. A synopsis of prostate organoid
635 methodologies, applications, and limitations. *Prostate* **80**, 518–526 (2020).
636 10. Maenhoudt, N. & Vankelecom, H. Protocol for establishing organoids from human
637 ovarian cancer biopsies. *STAR Protoc* **2**, 100429 (2021).
638 11. Gunti, S., Hoke, A. T. K., Vu, K. P. & London, N. R. Organoid and Spheroid
639 Tumor Models: Techniques and Applications. *Cancers (Basel)* **13**, 874 (2021).
640 12. Saito, Y. *et al.* Development of a functional thyroid model based on an organoid
641 culture system. *Biochem Biophys Res Commun* **497**, 783–789 (2018).
642 13. Chen, D. *et al.* Papillary thyroid cancer organoids harboring BRAFV600E
643 mutation reveal potentially beneficial effects of BRAF inhibitor-based
644 combination therapies. *J Transl Med* **21**, 9 (2023).
645 14. Vlachogiannis, G. *et al.* Patient-derived organoids model treatment response of
646 metastatic gastrointestinal cancers. *Science (1979)* **359**, 920–926 (2018).
647 15. Drost, J. *et al.* Sequential cancer mutations in cultured human intestinal stem cells.
648 *Nature* **521**, 43–47 (2015).
649 16. Matano, M. *et al.* Modeling colorectal cancer using CRISPR-Cas9–mediated
650 engineering of human intestinal organoids. *Nat Med* **21**, 256–262 (2015).
651 17. Miura, A. *et al.* Oncogenic potential of human pluripotent stem cell-derived lung
652 organoids with <scp>HER2</scp> overexpression. *Int J Cancer* **149**, 1593–1604
653 (2021).
654 18. Nadauld, L. D. *et al.* Metastatic tumor evolution and organoid modeling implicate
655 TGFBR2as a cancer driver in diffuse gastric cancer. *Genome Biol* **15**, 428 (2014).
656 19. Li, X. *et al.* Oncogenic transformation of diverse gastrointestinal tissues in primary
657 organoid culture. *Nat Med* **20**, 769–777 (2014).
658 20. Huang, L. *et al.* Ductal pancreatic cancer modeling and drug screening using
659 human pluripotent stem cell– and patient-derived tumor organoids. *Nat Med* **21**,
660 1364–1371 (2015).
661 21. Lo, Y.-H., Karlsson, K. & Kuo, C. J. Applications of organoids for cancer biology
662 and precision medicine. *Nat Cancer* **1**, 761–773 (2020).
663 22. Lim, H., Devesa, S. S., Sosa, J. A., Check, D. & Kitahara, C. M. Trends in Thyroid
664 Cancer Incidence and Mortality in the United States, 1974-2013. *JAMA* **317**, 1338
665 (2017).
666 23. ROMITTI, M. *et al.* Signaling pathways in follicular cell-derived thyroid
667 carcinomas. *Int J Oncol* **42**, 19–28 (2013).
668 24. Kimura, E. T. *et al.* High prevalence of BRAF mutations in thyroid cancer: genetic
669 evidence for constitutive activation of the RET/PTC-RAS-BRAF signaling
670 pathway in papillary thyroid carcinoma. *Cancer Res* **63**, 1454–7 (2003).
671 25. Fagin, J. A. & Mitsiades, N. Molecular pathology of thyroid cancer: diagnostic and
672 clinical implications. *Best Pract Res Clin Endocrinol Metab* **22**, 955–969 (2008).
673 26. Scheffel, R. S. *et al.* The BRAFV600E mutation analysis and risk stratification in
674 papillary thyroid carcinoma. *Arch Endocrinol Metab* (2020) doi:10.20945/2359-
675 3997000000285.
676 27. Xing, M. The T1799A BRAF mutation is not a germline mutation in familial
677 nonmedullary thyroid cancer. *Clin Endocrinol (Oxf)* **63**, 263–266 (2005).
678 28. Chakravarty, D. *et al.* Small-molecule MAPK inhibitors restore radioiodine
679 incorporation in mouse thyroid cancers with conditional BRAF activation. *Journal
680 of Clinical Investigation* **121**, 4700–4711 (2011).
681 29. Zaman, Wu & Bivona. Targeting Oncogenic BRAF: Past, Present, and Future.
682 *Cancers (Basel)* **11**, 1197 (2019).

683 30. Agrawal, N. *et al.* Integrated Genomic Characterization of Papillary Thyroid
684 Carcinoma. *Cell* **159**, 676–690 (2014).
685 31. Romei, C. *et al.* Modifications in the Papillary Thyroid Cancer Gene Profile Over
686 the Last 15 Years. *J Clin Endocrinol Metab* **97**, E1758–E1765 (2012).
687 32. Sabra, M. M. *et al.* Clinical Outcomes and Molecular Profile of Differentiated
688 Thyroid Cancers With Radioiodine-Avid Distant Metastases. *J Clin Endocrinol*
689 *Metab* **98**, E829–E836 (2013).
690 33. Xing, M. BRAFV600E Mutation and Papillary Thyroid Cancer. *JAMA* **310**, 535
691 (2013).
692 34. Scheffel, R. S. *et al.* The BRAFV600E mutation analysis and risk stratification in
693 papillary thyroid carcinoma. *Arch Endocrinol Metab* (2021) doi:10.20945/2359-
694 3997000000285.
695 35. Liu, R. *et al.* Mortality Risk Stratification by Combining *BRAF* V600E and *TERT*
696 Promoter Mutations in Papillary Thyroid Cancer. *JAMA Oncol* **3**, 202 (2017).
697 36. Boucai, L. *et al.* Characterization of Subtypes of BRAF-Mutant Papillary Thyroid
698 Cancer Defined by Their Thyroid Differentiation Score. *J Clin Endocrinol Metab*
699 **107**, 1030–1039 (2022).
700 37. Antonica, F. *et al.* Generation of functional thyroid from embryonic stem cells.
701 *Nature* **491**, 66–71 (2012).
702 38. Romitti, M. *et al.* Transplantable human thyroid organoids generated from
703 embryonic stem cells to rescue hypothyroidism. *Nat Commun* **13**, 7057 (2022).
704 39. Longmire, T. A. *et al.* Efficient derivation of purified lung and thyroid progenitors
705 from embryonic stem cells. *Cell Stem Cell* **10**, 398–411 (2012).
706 40. Ma, R., Latif, R. & Davies, T. F. Human embryonic stem cells form functional
707 thyroid follicles. *Thyroid* **25**, 455–461 (2015).
708 41. Ma, R., Latif, R. & Davies, T. F. Thyroid follicle formation and thyroglobulin
709 expression in multipotent endodermal stem cells. *Thyroid* **23**, 385–391 (2013).
710 42. Ma, R., Morshed, S. A., Latif, R. & Davies, T. F. TAZ Induction Directs
711 Differentiation of Thyroid Follicular Cells from Human Embryonic Stem Cells.
712 *Thyroid* **27**, 292–299 (2017).
713 43. Ma, R., Shi, R., Morshed, S. A., Latif, R. & Davies, T. F. Derivation and 97%
714 Purification of Human Thyroid Cells From Dermal Fibroblasts. *Front Endocrinol*
715 *(Lausanne)* **11**, 446 (2020).
716 44. Kurmann, A. A. *et al.* Regeneration of Thyroid Function by Transplantation of
717 Differentiated Pluripotent Stem Cells. *Cell Stem Cell* **17**, 527–542 (2015).
718 45. Serra, M. *et al.* Pluripotent stem cell differentiation reveals distinct developmental
719 pathways regulating Lung-Versus Thyroid-Lineage specification. *Development*
720 *(Cambridge)* **144**, 3879–3893 (2017).
721 46. Dame, K. *et al.* Thyroid Progenitors Are Robustly Derived from Embryonic Stem
722 Cells through Transient, Developmental Stage-Specific Overexpression of Nkx2-
723 1. *Stem Cell Reports* **8**, 216–225 (2017).
724 47. Ogundipe, V. M. L. *et al.* Generation and Differentiation of Adult Tissue-Derived
725 Human Thyroid Organoids. *Stem Cell Reports* **16**, 913–925 (2021).
726 48. Liang, J. *et al.* Modeling Human Thyroid Development by Fetal Tissue-Derived
727 Organoid Culture. *Advanced Science* **9**, (2022).
728 49. van der Vaart, J. *et al.* Adult mouse and human organoids derived from thyroid
729 follicular cells and modeling of Graves' hyperthyroidism. *Proceedings of the*
730 *National Academy of Sciences* **118**, (2021).
731 50. Chen, D. *et al.* Organoid Cultures Derived From Patients With Papillary Thyroid
732 Cancer. *J Clin Endocrinol Metab* **106**, 1410–1426 (2021).

733 51. Sondorp, L. H. J. *et al.* Patient-Derived Papillary Thyroid Cancer Organoids for
734 Radioactive Iodine Refractory Screening. *Cancers (Basel)* **12**, 3212 (2020).
735 52. Pecce, V. *et al.* Establishment and maintenance of thyroid organoids from human
736 cancer cells. *STAR Protoc* **3**, 101393 (2022).
737 53. Chen, D. *et al.* Papillary thyroid cancer organoids harboring BRAFV600E
738 mutation reveal potentially beneficial effects of BRAF inhibitor-based
739 combination therapies. *J Transl Med* **21**, 9 (2023).
740 54. Yang, H. *et al.* Establishment of papillary thyroid cancer organoid lines from
741 clinical specimens. *Front Endocrinol (Lausanne)* **14**, (2023).
742 55. Veschi, V. *et al.* Recapitulating thyroid cancer histotypes through engineering
743 embryonic stem cells. *Nat Commun* **14**, 1351 (2023).
744 56. Haenebalcke, L. *et al.* Efficient ROSA26-Based Conditional and/or Inducible
745 Transgenesis Using RMCE-Compatible F1 Hybrid Mouse Embryonic Stem Cells.
746 *Stem Cell Rev Rep* **9**, 774–785 (2013).
747 57. Romitti, M. *et al.* Single-Cell Trajectory Inference Guided Enhancement of
748 Thyroid Maturation In Vitro Using TGF-Beta Inhibition. *Front Endocrinol*
749 *(Lausanne)* **12**, (2021).
750 58. Ortiz, O., Wurst, W. & Kühn, R. Reversible and tissue-specific activation of MAP
751 kinase signaling by tamoxifen in braf ^{V637} ER ^{T2} mice. *genesis* **51**, 448–455 (2013).
752 59. Azouzi, N. *et al.* NADPH Oxidase NOX4 Is a Critical Mediator of BRAF ^{V600E} -
753 Induced Downregulation of the Sodium/Iodide Symporter in Papillary Thyroid
754 Carcinomas. *Antioxid Redox Signal* **26**, 864–877 (2017).
755 60. Kogai, T. & Brent, G. A. The sodium iodide symporter (NIS): Regulation and
756 approaches to targeting for cancer therapeutics. *Pharmacol Ther* **135**, 355–370
757 (2012).
758 61. Bolger, A. M., Lohse, M. & Usadel, B. Trimmomatic: a flexible trimmer for
759 Illumina sequence data. *Bioinformatics* **30**, (2014).
760 62. Kim, D., Langmead, B. & Salzberg, S. L. HISAT: a fast spliced aligner with low
761 memory requirements. *Nat Methods* **12**, (2015).
762 63. Hao, Y. *et al.* Integrated analysis of multimodal single-cell data. *Cell* **184**, 3573-
763 3587.e29 (2021).
764 64. Love, M. I., Huber, W. & Anders, S. Moderated estimation of fold change and
765 dispersion for RNA-seq data with DESeq2. *Genome Biol* **15**, 550 (2014).
766 65. Dunn, L. A. *et al.* Vemurafenib Redifferentiation of *BRAF* Mutant, RAI-
767 Refractory Thyroid Cancers. *J Clin Endocrinol Metab* **104**, 1417–1428 (2019).
768 66. Tang, W.-W., Huang, C., Tang, C., Xu, J. & Wang, H. Galectin-3 may serve as a
769 potential marker for diagnosis and prognosis in papillary thyroid carcinoma: a
770 meta-analysis. *Onco Targets Ther* 455 (2016) doi:10.2147/OTT.S94514.
771 67. Xia, S. *et al.* Fibronectin 1 promotes migration and invasion of papillary thyroid
772 cancer and predicts papillary thyroid cancer lymph node metastasis. *Onco Targets*
773 *Ther* **Volume 10**, 1743–1755 (2017).
774 68. Sponziello, M. *et al.* Fibronectin-1 expression is increased in aggressive thyroid
775 cancer and favors the migration and invasion of cancer cells. *Mol Cell Endocrinol*
776 **431**, 123–132 (2016).
777 69. Knauf, J. A. *et al.* Targeted Expression of BRAFV600E in Thyroid Cells of
778 Transgenic Mice Results in Papillary Thyroid Cancers that Undergo
779 Dedifferentiation. *Cancer Res* **65**, 4238–4245 (2005).
780 70. Saqcena, M. *et al.* SWI/SNF Complex Mutations Promote Thyroid Tumor
781 Progression and Insensitivity to Redifferentiation Therapies. *Cancer Discov* **11**,
782 1158–1175 (2021).

783 71. Qiu, W., Yang, Z., Fan, Y. & Zheng, Q. ZNRF3 is downregulated in papillary
784 thyroid carcinoma and suppresses the proliferation and invasion of papillary
785 thyroid cancer cells. *Tumor Biology* **37**, 12665–12672 (2016).
786 72. Han, J. *et al.* Identification of Biomarkers Based on Differentially Expressed
787 Genes in Papillary Thyroid Carcinoma. *Sci Rep* **8**, 9912 (2018).
788 73. Yoo, S.-K. *et al.* Integrative analysis of genomic and transcriptomic characteristics
789 associated with progression of aggressive thyroid cancer. *Nat Commun* **10**, 2764
790 (2019).
791 74. Davies, H. *et al.* Mutations of the BRAF gene in human cancer. *Nature* **417**, 949–
792 954 (2002).
793 75. Dhomen, N. & Marais, R. New insight into BRAF mutations in cancer. *Curr Opin*
794 *Genet Dev* **17**, 31–39 (2007).
795 76. Nikiforov, Y. E. & Nikiforova, M. N. Molecular genetics and diagnosis of thyroid
796 cancer. *Nat Rev Endocrinol* **7**, 569–580 (2011).
797 77. Cheng, L., Lopez-Beltran, A., Massari, F., MacLennan, G. T. & Montironi, R.
798 Molecular testing for BRAF mutations to inform melanoma treatment decisions: a
799 move toward precision medicine. *Modern Pathology* **31**, 24–38 (2018).
800 78. Schirripa, M. *et al.* Class 1, 2, and 3 BRAF-Mutated Metastatic Colorectal Cancer:
801 A Detailed Clinical, Pathologic, and Molecular Characterization. *Clinical Cancer*
802 *Research* **25**, 3954–3961 (2019).
803 79. Pisapia, P., Pepe, F., Malapelle, U. & Troncone, G. Mutations in Lung Cancer.
804 *Acta Cytol* **63**, 247–250 (2019).
805 80. Pisapia, P. *et al.* BRAF: A Two-Faced Janus. *Cells* **9**, 2549 (2020).
806 81. Pavlick, A. C., Fecher, L., Ascierto, P. A. & Sullivan, R. J. Frontline Therapy for
807 BRAF-Mutated Metastatic Melanoma: How Do You Choose, and Is There One
808 Correct Answer? *American Society of Clinical Oncology Educational Book* 564–
809 571 (2019) doi:10.1200/EDBK_243071.
810 82. Anguera, G. & Majem, M. BRAF inhibitors in metastatic non-small cell lung
811 cancer. *J Thorac Dis* **10**, 589–592 (2018).
812 83. Haugen, B. R. *et al.* 2015 American Thyroid Association Management Guidelines
813 for Adult Patients with Thyroid Nodules and Differentiated Thyroid Cancer: The
814 American Thyroid Association Guidelines Task Force on Thyroid Nodules and
815 Differentiated Thyroid Cancer. *Thyroid* **26**, 1–133 (2016).
816 84. Schmidbauer, B., Menhart, K., Hellwig, D. & Grosse, J. Differentiated Thyroid
817 Cancer—Treatment: State of the Art. *Int J Mol Sci* **18**, 1292 (2017).
818 85. Kim, T. Y., Kim, W. G., Kim, W. B. & Shong, Y. K. Current Status and Future
819 Perspectives in Differentiated Thyroid Cancer. *Endocrinology and Metabolism* **29**,
820 217 (2014).
821 86. Ahn, B.-C. Personalized Medicine Based on Theranostic Radioiodine Molecular
822 Imaging for Differentiated Thyroid Cancer. *Biomed Res Int* **2016**, 1–9 (2016).
823 87. Paeng, J. C., Kang, K. W., Park, D. J., Oh, S. W. & Chung, J.-K. Alternative
824 Medical Treatment for Radioiodine-Refractory Thyroid Cancers. *Nucl Med Mol*
825 *Imaging* **45**, 241–247 (2011).
826 88. Brose, M. S. *et al.* Sorafenib in radioactive iodine-refractory, locally advanced or
827 metastatic differentiated thyroid cancer: a randomised, double-blind, phase 3 trial.
828 *The Lancet* **384**, 319–328 (2014).
829 89. Schlumberger, M. *et al.* Lenvatinib versus Placebo in Radioiodine-Refractory
830 Thyroid Cancer. *New England Journal of Medicine* **372**, 621–630 (2015).
831 90. Ho, A. L. *et al.* Selumetinib-Enhanced Radioiodine Uptake in Advanced Thyroid
832 Cancer. *New England Journal of Medicine* **368**, 623–632 (2013).

91. Rothenberg, S. M., Daniels, G. H. & Wirth, L. J. Redifferentiation of Iodine-Refractory BRAF V600E-Mutant Metastatic Papillary Thyroid Cancer with Dabrafenib—Response. *Clinical Cancer Research* **21**, 5640–5641 (2015).
92. Buffet, C. *et al.* Redifferentiation of radioiodine-refractory thyroid cancers. *Endocr Relat Cancer* **27**, R113–R132 (2020).
93. Riesco-Eizaguirre, G. & Santisteban, P. A perspective view of sodium iodide symporter research and its clinical implications. *Eur J Endocrinol* **155**, 495–512 (2006).
94. Czarnecka, A. M., Bartnik, E., Fiedorowicz, M. & Rutkowski, P. Targeted Therapy in Melanoma and Mechanisms of Resistance. *Int J Mol Sci* **21**, 4576 (2020).
95. Flaherty, K. T. *et al.* Combined BRAF and MEK Inhibition in Melanoma with BRAF V600 Mutations. *New England Journal of Medicine* **367**, 1694–1703 (2012).
96. Larkin, J. *et al.* Combined Vemurafenib and Cobimetinib in BRAF-Mutated Melanoma. *New England Journal of Medicine* **371**, 1867–1876 (2014).
97. Dummer, R. *et al.* Encorafenib plus binimetinib versus vemurafenib or encorafenib in patients with BRAF -mutant melanoma (COLUMBUS): a multicentre, open-label, randomised phase 3 trial. *Lancet Oncol* **19**, 603–615 (2018).
98. Smalley, K. S. M. Increased immunity and BRAF inhibition: Yet another argument for combination therapy? *Pharmacol Res* **113**, 719–720 (2016).
99. Roskoski, R. Targeting oncogenic Raf protein-serine/threonine kinases in human cancers. *Pharmacol Res* **135**, 239–258 (2018).

869 **Figures**

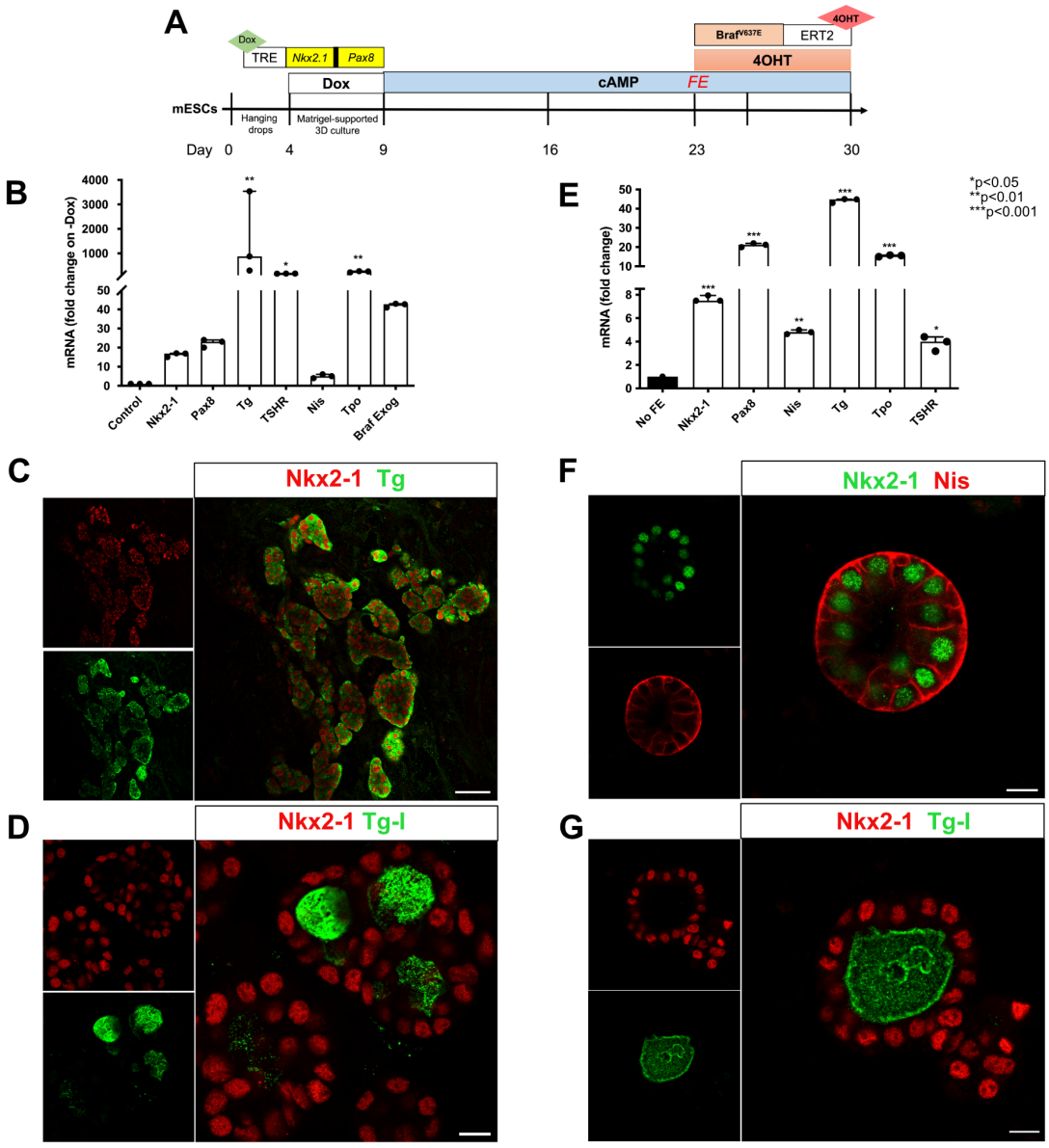

870

871 **Figure 1. mESC_Nkx2-1/Pax8_bTg_Braf^{V637E} cell line differentiation into thyroid**
872 **organoids.** Scheme of the thyroid differentiation protocol and Braf^{V637E} induction in
873 mature thyroid follicles (A). Differentiation of mESC_Nkx2-1/Pax8_bTg_Braf^{V637E} cell
874 line promotes expression of the main thyroid genes and Braf exogenous (B).
875 Immunofluorescence staining showing Nkx2-1 and Tg co-expressing cells organized in
876 follicular structures (C) which are accumulating the thyroid hormone precursor, Tg-I,
877 inside the lumen compartment (D). Follicular enrichment (FE) procedure significantly
878 increased the expression levels of thyroid genes (E) while kept the structural organization

879 of the follicles (F) and its functionality evidenced by Tg-I accumulation (G). Scale bars,

880 50 µm and 10 µm for high magnification follicles.

881

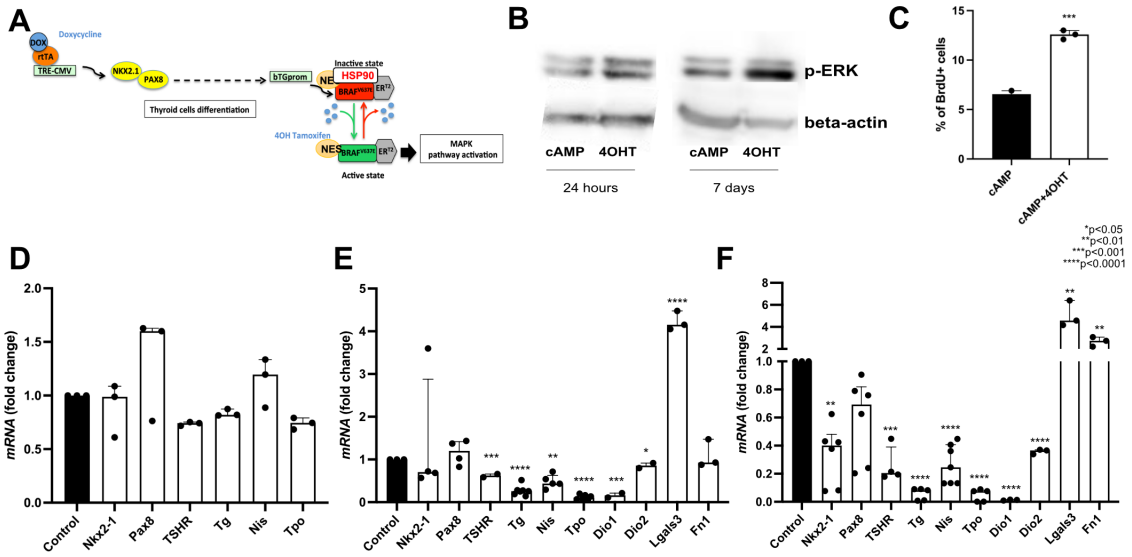

882

883 **Figure 2. Effect of the Braf^{V637E} oncogene induction on mature thyroid follicles.**

884 Schematic representation of thyroid differentiation, Braf^{V637E} oncogene expression and

885 its activation under specific treatment conditions (A). Western blot demonstrates increase

886 of p-ERK protein at 24 hours and 7 days after addition of 4OHT (Tamoxifen) to the

887 organoids culture (B). Percentage of BrDU+ cells between control (cAMP) and Braf-

888 induced (4OHT; 6 days) condition (C). mRNA expression analysis showing the inhibitory

889 effect of Braf^{V637E}-oncogene induction on thyroid genes after 6 hours (D), 48 hours (E)

890 and 7 days (F).

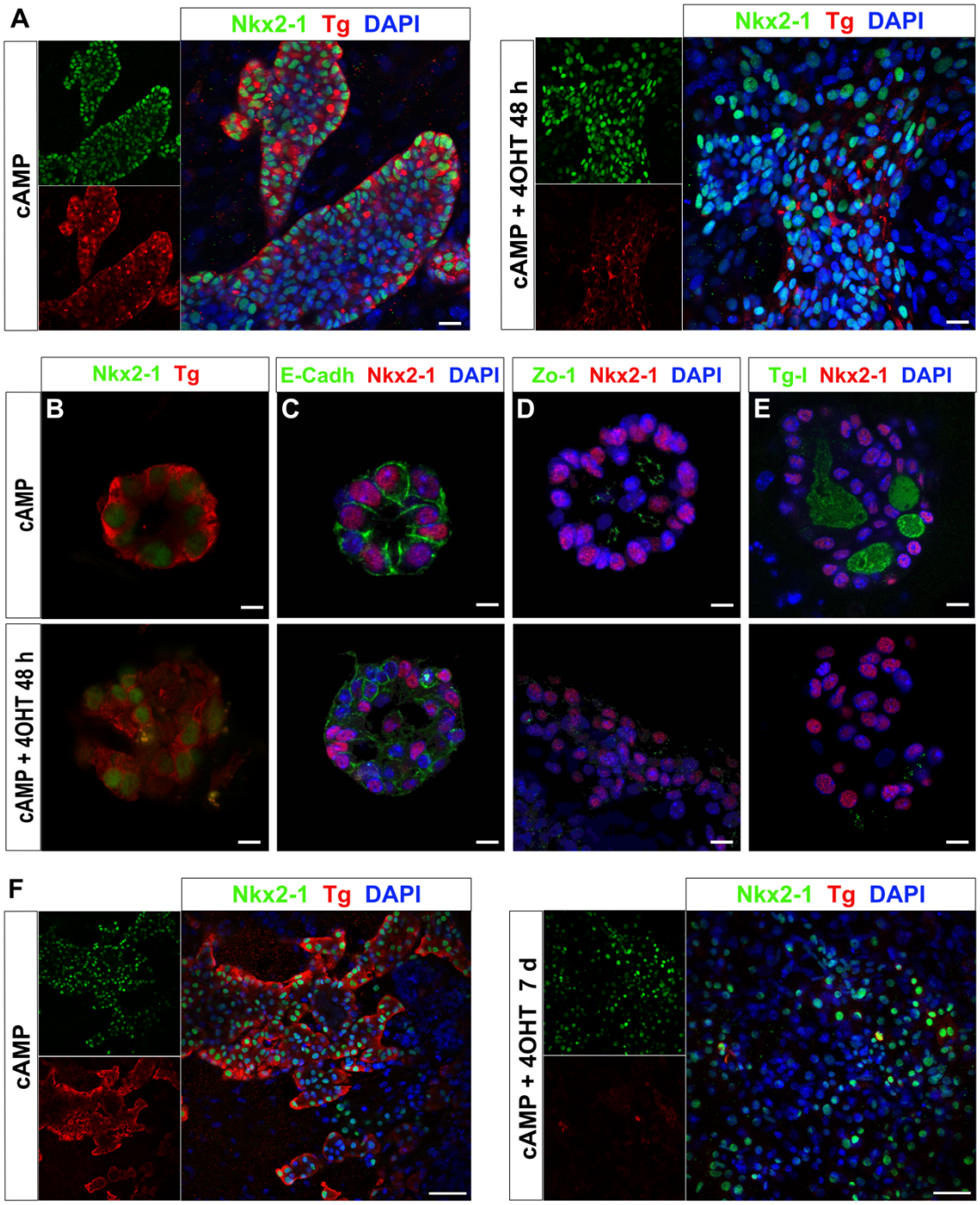

Figure 3. Morphological changes caused by Braf^{V637E} activation on thyroid follicles. Control thyroid cells showing follicular organization with Nkx2-1 nuclear expression and Tg accumulation in the luminal compartment while after 48 h of Braf oncogene induction by 4OHT most of the cells are not organized into follicular structures and a great proportion of cells is expressing very low levels of Tg (A). Higher magnification images showing the follicular organization of the thyroid cells in the control condition (48 h),

898 with proper expression of Nk2x-1 and/or Tg (B), E-cadherin (C), Zo-1 (D) and Tg-I (E)
899 accumulation in the lumen. While in the 4OHT condition the follicular organization is
900 disrupted as well as its function. Nkx2-1 and Tg staining in control and Braf-induced cells
901 for 7 days shows clear changes in thyroid morphology evidenced by the heterogeneity of
902 Nkx2-1 cells which mostly do not express Tg or at low levels, while some groups cells
903 continue to co-express Tg (F). Scale bars, 20 µm (A), 10 µm (B-E) and 50 µm (F).
904

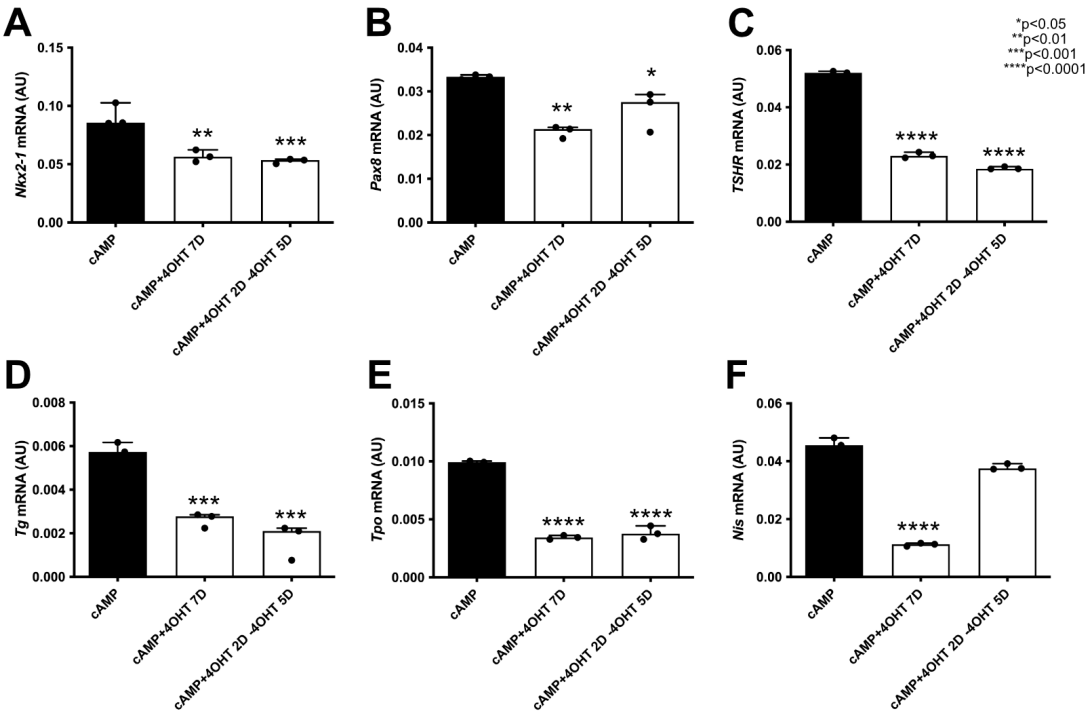

905

906 **Figure 4. 4OHT interruption does not restores the thyroid gene expression levels.**
907 The induction of Braf^{V637E} for 2 days followed by removal of 4OHT for 5 days shows
908 that it is not enough to recover the levels of *Nkx2-1* (A), *Pax8* (B), *TSHR* (C), *Tg* (D), *Tpo*
909 (E) genes to the control levels. However, it led to increase of *Nis* expression (F) close to
910 control values.

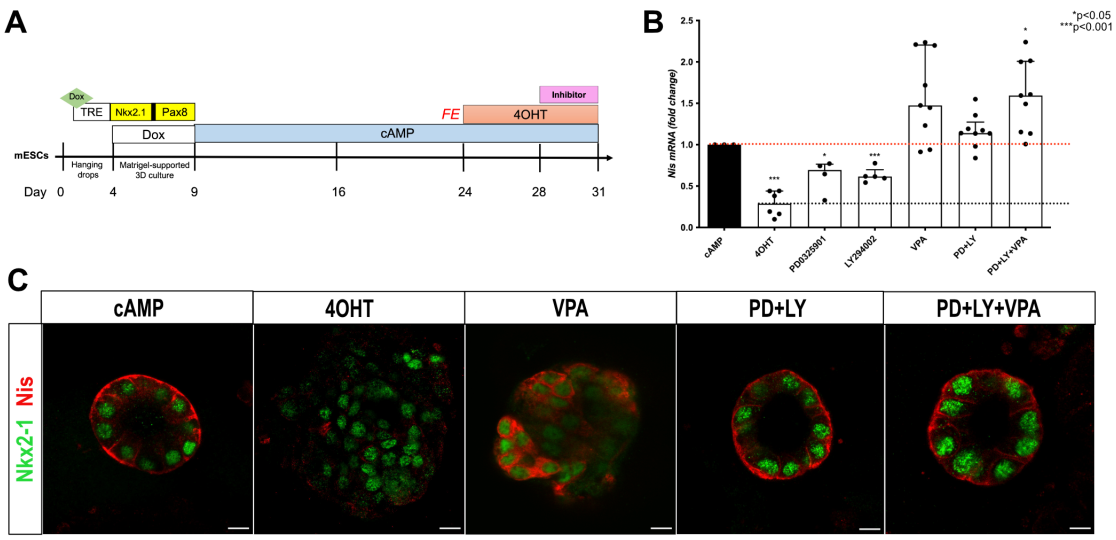

Figure 5. Drug screening reveals that VPA and MAPK/PI3K inhibition can restore Nis expression in Braf-induced cells. Schematic representation of the protocol used for drug screening experiments (A). qPCR data shows that inhibition of MAPK (PD0325901) and PI3K (LY294002) pathways isolated increase but do not restore *Nis* expression to control levels. However, when combined, the levels are like the controls. On the other hand, the HDAC inhibitor (VPA) can, by itself, recover *Nis* expression (B). Nkx2-1 and Nis immunostaining show the downregulation of the transporter in 4OHT condition, which is restored by VPA treatment. However, the expression pattern differs from the control conditions. Co-inhibition of MAPK and PI3K pathways associated or not to VPA treatment restores of Nis protein expression while follicular structures are observed (C). Scale bars, 10 µm.

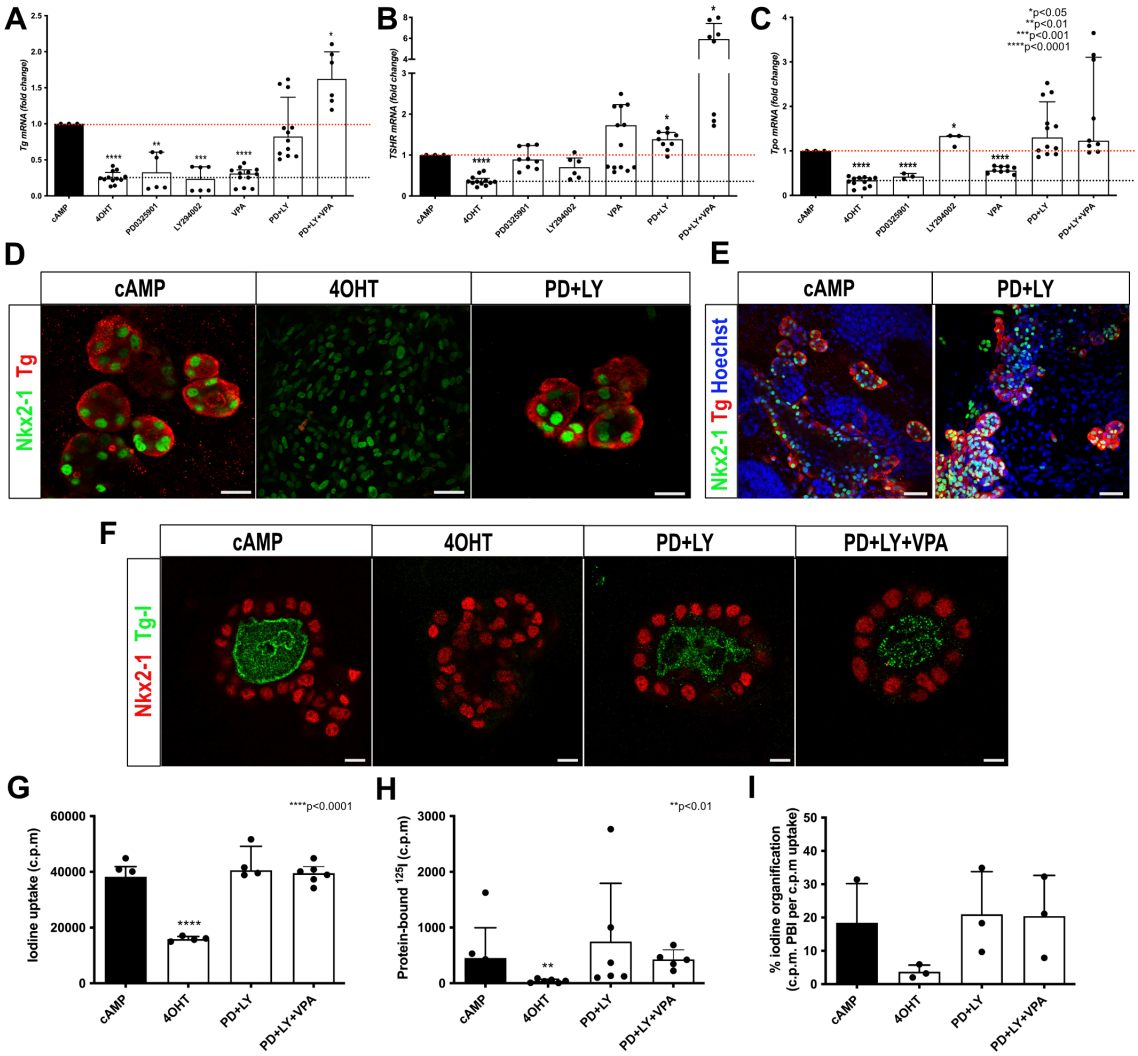

924

925 **Figure 6. MAPK and PI3K inhibition cause thyroid redifferentiation and function**
926 **recovery of Braf-expressing cells.** mRNA expression analysis showing that PD0325901
927 and LY294002 co-treatment recover the *Tg* (A), *TSHR* (B) and *Tpo* (C) gene expression
928 to control levels. Immunostaining for Nkx2-1 and Tg shows that proteins levels are
929 similar to control and that follicular organization is restored under such treatment
930 condition (D, E). Tg-I accumulation in the lumen of the restored follicles is observed
931 under PD+LY and PD+LY+VPA conditions (F). Organification assay shows recovery of
932 Iodine uptake (G), Protein-bound to 125I (H) and % of iodine Organification (I) in the
933 inhibitor's conditions. Scale bars, 50 µm (E), 20 µm (D) and 10 µm for high magnification
934 follicles (F).

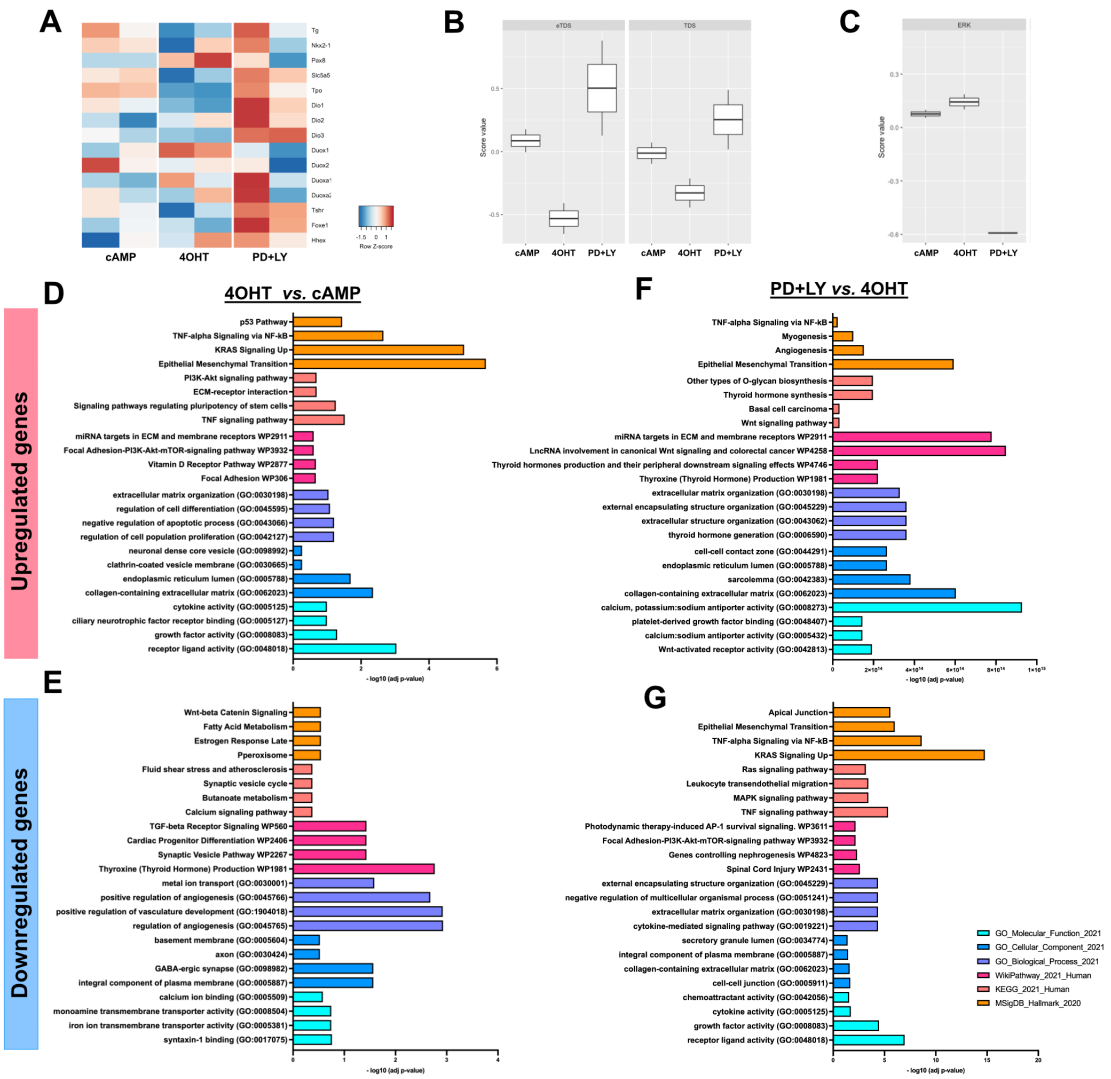

Figure 7. Transcriptomics analysis confirms thyroid redifferentiation of Braf^{V637E}-expressing cells treated with MAPK and PI3K inhibitors and suggests by which mechanisms. Heatmap of normalized bulk RNA-Seq expression of normal thyroid cells (cAMP), Braf^{V637E} expressing cells (4OHT) and Braf^{V637E} expressing cells treated with PD0325901+LY204002 inhibitors. Rows represent markers and columns represent specific conditions. Color values in the heatmap represent mean expression levels (A). Thyroid differentiation (eTDS and TDS) (B) and ERK (C) scores calculated among the different conditions. Classification of upregulated and downregulated genes comparing 4OHT *vs.* cAMP (D, E) and PD+LY *vs.* 4OHT (F, G). Colours represent the classification method and scale the -log10 (adj p-value).

946 **Supplementary data**

947

948 Supplementary figures

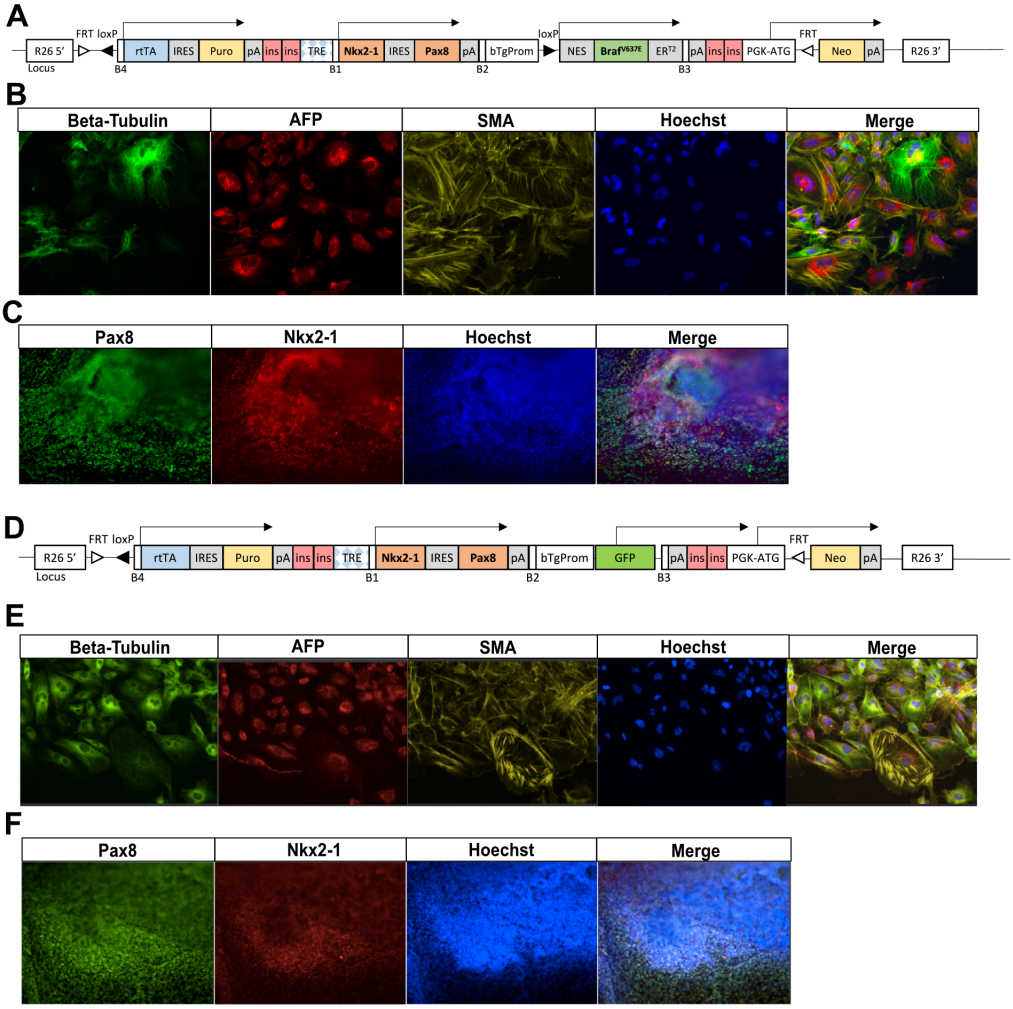

949

950 **Figure S1. mESC-cell lines generation and characterization.** Schematic representation
951 of the mESC_Nkx2-1/Pax8_bTg_Braf^{V637E} cell line (A). mESC_Nkx2-
952 1/Pax8_bTg_Braf^{V637E} line response to doxycycline treatment shows expression of Pax8
953 and Nkx2-1 proteins (B). Spontaneous differentiation mESC_Nkx2-
954 1/Pax8_bTg_Braf^{V637E} cell line leads to generation of ectodermal (Beta-actin),
955 endodermal (AFP) and mesodermal (SMA) cells (C). Schematic representation of the
956 mESC_Nkx2-1/Pax8_bTg_eGFP control cell line (D). Dox treatment leads to increase of
957 Pax8 and Nkx2-1 expression in control cells (E). Spontaneous differentiation of the

958 control cells leads to generation of ectodermal (Beta-actin), endodermal (AFP) and
959 mesodermal (SMA) cells (F). Scale bars, 50 µm (B, E) and 10 µm (C, F).
960

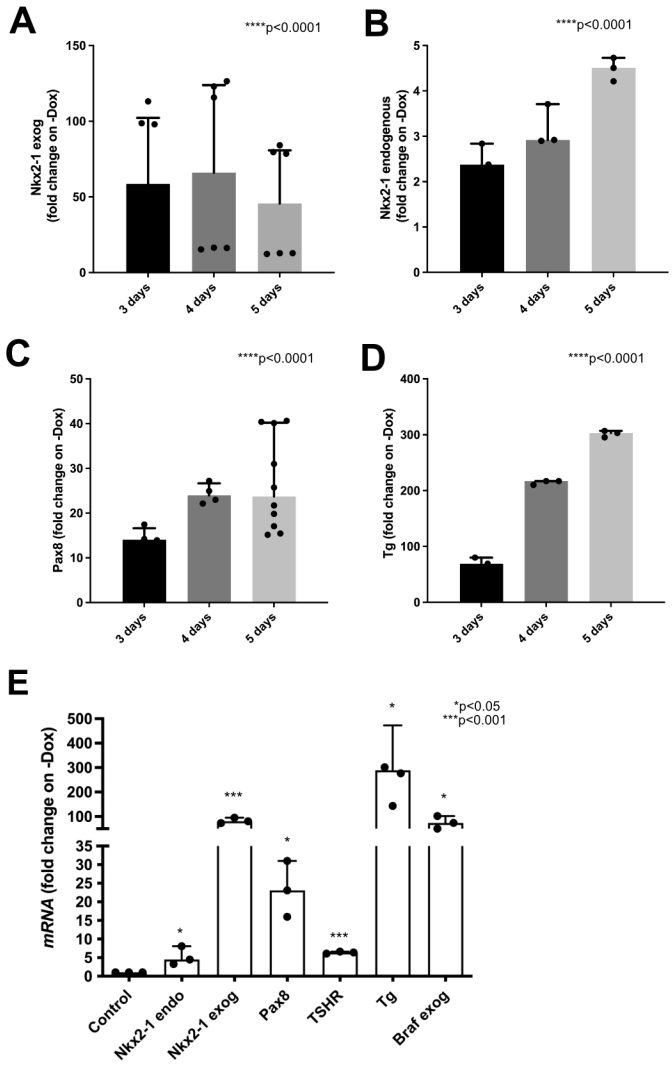

961

962 **Figure S2. Doxycycline treatment for 5 days leads to more efficient thyroid genes**
963 **expression induction.** Time course of Dox-dependent induction of exogenous and
964 endogenous *Nkx2-1* (A, B) *Pax8* (C) and *Tg* (D) expression. mRNA levels of thyroid
965 genes at day 9, after 5 days of Dox treatment (E).

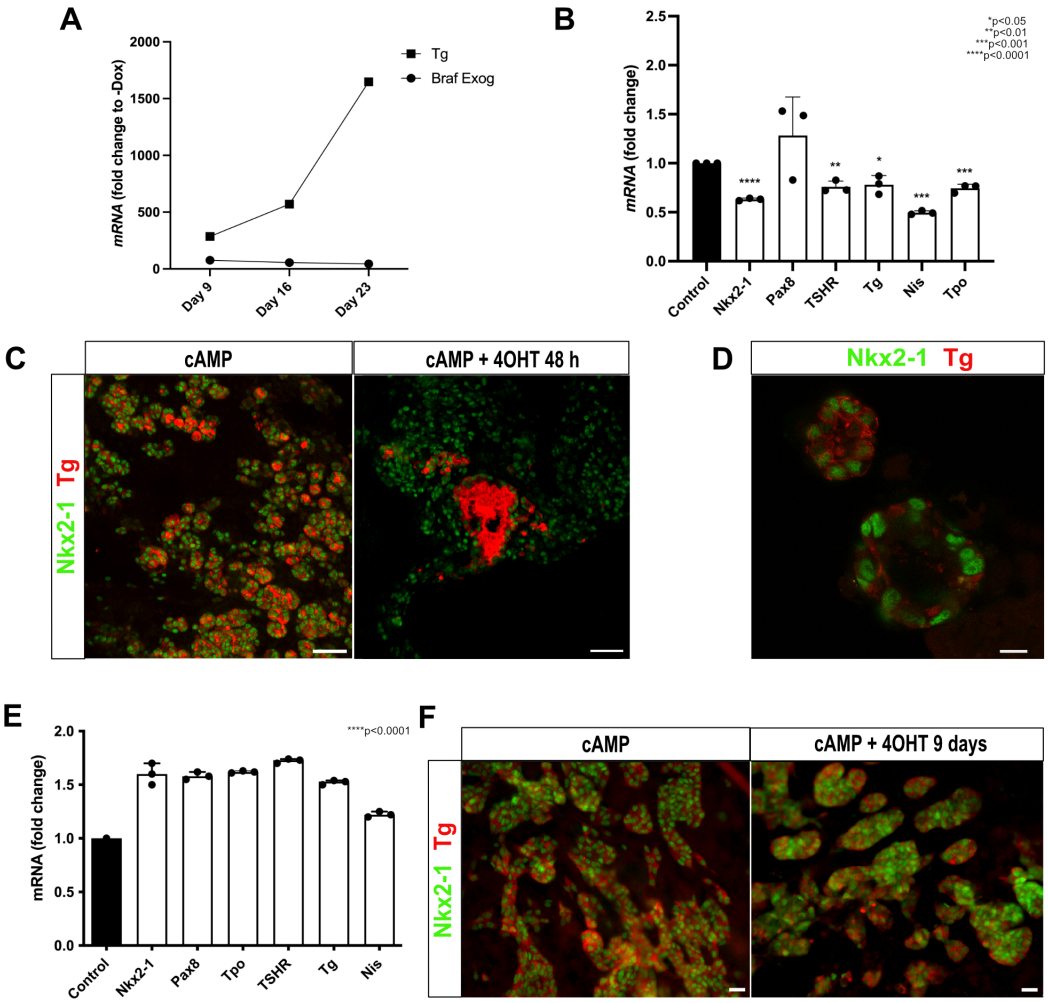

Figure S3. 4OHT treatment rapidly induces Braf-carcinogenic changes in gene expression and follicular organization. Tg and Braf exogenous expression levels at day 9, 16 and 23 of thyroid differentiation protocol (A). Induction of Braf^{V637E} for 8 hours promotes downregulation of main thyroid genes (B). Nkx2-1 and Tg immunostaining shows that under BrafV637E activation (4OHT; 48 h) thyroid follicles present bigger size heterogeneous distribution of Tg compared to the control (C). Remaining follicular-like structures after Braf^{V637E} activation (4OHT; 48 h) (D). mRNA expression of mESC-Nkx2-1-Pax8_bTg-eGFP derived follicles treated for 9 days with 4OHT (E). Nkx2-1 and Tg co-staining demonstrate that 4OHT treatment do not affect thyroid organization (F). Scale bars, 50 µm (C), 20 µm (F) and 10 µm (D).

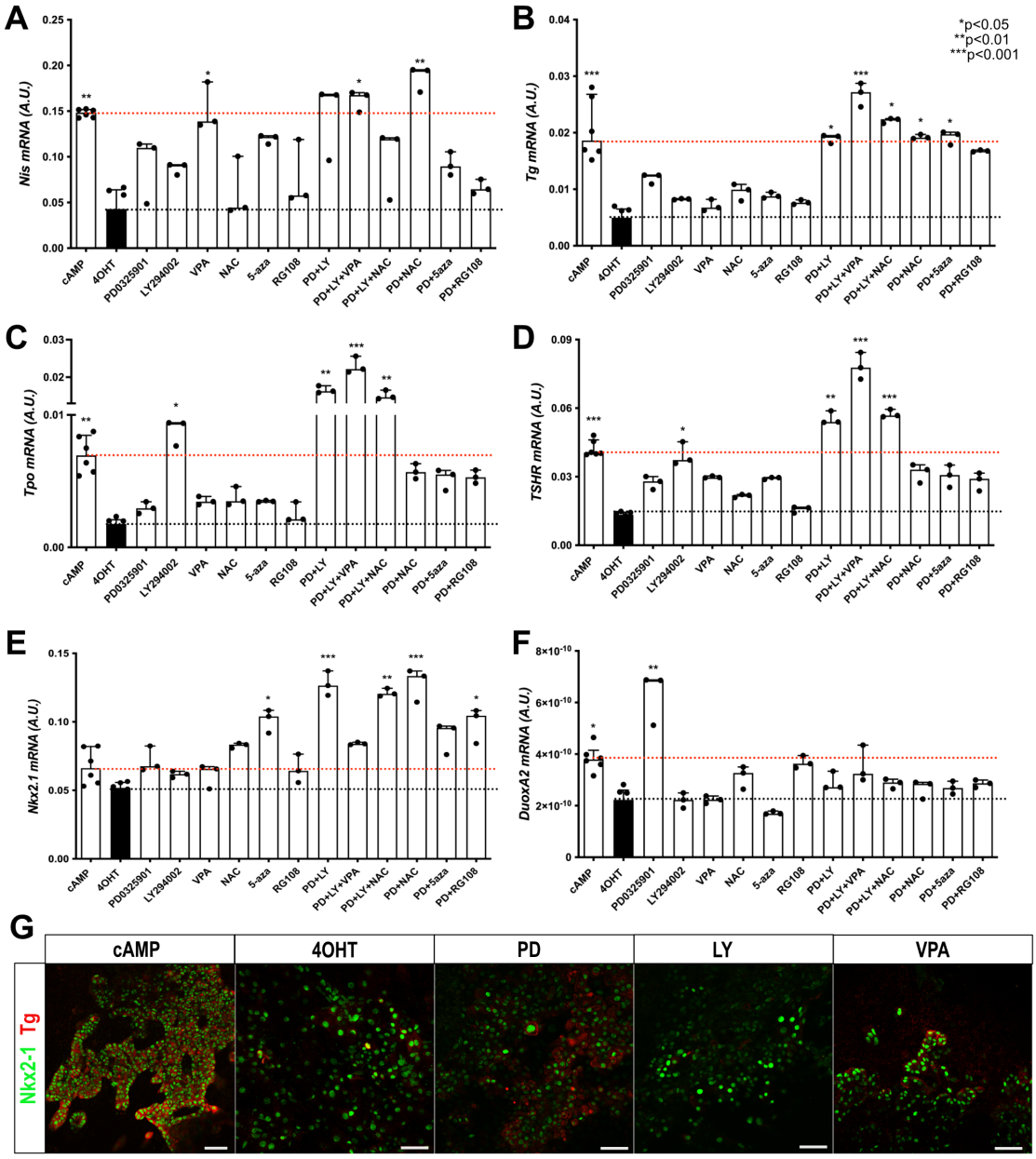

Figure S4. Effect of distinct classes of inhibitors on thyroid markers. Gene expression levels of *Nis* (A), *Tg* (B), *Tpo* (C), *TSHR* (D), *Nkx2.1* (E) *and Duox2A* (F) among normal thyroid organoids, Braf^{V637E}-expressing (4OHT) and treated with distinct inhibitor (4OHT+inhib). Significance is compared to 4OHT condition. Nkx2-1 and Tg co-staining shows that PD0325901, LY294002 and VPA treatments isolated is not enough to revert the inhibitory effect of Braf^{V637E} activation on Tg expression and thyroid follicular organization. Scale bar, 50 µm.

986 **Supplementary tables**

987

988 **Supplementary Table 1.** Antibodies information.

Primary antibodies						
Protein Target	***Provider***	***Catalog number***	***Host Species***	***Dilution Flow Cyt.***	***Dilution IF***	***Dilution WB***
AFP	Santa Cruz	sc-8108	Goat		1:100	
β-III Tubulin	Eurogentec	MMS-435P-200	Mouse		1:1,000	
αSMA	Abcam	ab32575	Rabbit		1:1,000	
Nkx2-1	Abcam	ab76013	Rabbit	1 :100	1:500	
PAX8	Cell Signaling	59019	Rabbit		1:500	
Tg	Dako	A0251	Rabbit		1:2,000	
Tg	Abcam	Ab187378	Mouse		1:250	
Nis	Gift from N. Carrasco		Rabbit		1:1,000	
TG-I	Gift from C. Ris-Stalpers		Mouse		1:250	
E-cadherin	BD	610181	Mouse		1:1,000	
ZO-1	Invitrogen	339100	Mouse		1:500	
Hoechst	Invitrogen	33342			1:1,000	
p-ERK	Cell Signaling	4370	Rabbit			1:1,000
β-Actin	Cell Signaling	3700	Mouse			1:1,000
Secondary antibodies						
Cy3-conjugated	Jackson Immunoresearch	715-165-150	Donkey anti-mouse IgG		1:500	
Cy3-conjugated	Jackson Immunoresearch	711-165-152	Donkey anti-rabbit IgG		1:500	

Cy3-conjugated	Jackson Immunoresearch	705-165-147	Donkey anti-goat IgG		1:500	
Alexa fluor 488-conjugated	Jackson Immunoresearch	715-545-150	Donkey anti-mouse IgG		1:500	
Alexa fluor 647-conjugated	Jackson Immunoresearch	715-605-150	Donkey anti-mouse IgG		1:500	
Alexa fluor 647-conjugated	Jackson Immunoresearch	711-605-152	Donkey anti-rabbit IgG	1:300	1:500	
Anti-rabbit IgG, HRP-linked	Cell Signaling	7074				1:1,000
Anti-mouse IgG, HRP-linked	Cell Signaling	7076				1:1,000

989

990 **Supplementary Table 2.** List of primers used for RT-qPCR analysis.

Gene	**Primer Forward**	**Primer Reverse**
β2m-Globulin	GCTTCAGTCGTCAGCATGG	CAGTTCAGTATGTTCGGCTTCC
Nkx2-1 exog.	GGCGCCATGTCTTGTTCT	ACACCGGCCTTATTCCAAG
Nkx2-1	GGCGCCATGTCTTGTTCT	GGGCTCAAGCGCATCTCA
Pax8	CAGCCTGCTGAGTTCTCCAT	CTGTCTCAGGCCAAGTCCTC
Foxe1	GGCGGCATCTACAAGTTCAT	GGATCTTGAGGAAGCAGTCG
Tg	GTCCAATGCCAAAATGATGGTC	GAGAGCATCGGTGCTGTTAAT
Nis/Slc5a5	AGCTGCCAACACTTCCAGAG	GATGAGAGCACCACAAAGCA
Tshr	GTCTGCCCAATATTTCCAGGATCTA	GCTCTGTCAAGGCATCAGGGT
Tpo	ACAGTCACAGTTCTCCACGGATG	ATCTCTATTGTTGCACGCCCC
Braf exog.	GCTTGTGCTTCTCCGAAAAC	AAGGCCAGGCTGTTCTTCTT
Dio1	ATGGCCAGGAACCCCCG	GCCTGCTGCCTTGAATGAAA
Dio2	TTCTCCAACTGCCTCTTCCTG	CCCATCAGCGGTCTTCTCC
Gal3	TTGAAGCTGACCACTTCAAGGTT	AGGTTCTTCATCCGATGGTTGT
Fn1	AATCACAGTAGTTGCGGCAGGAGA	TCTGTCCCAGGCAGGAGATTTGTT

991

992 **Supplementary Table 3.** Gene list used for thyroid differentiation (TDS and eTDS) and

993 ERK scores calculation.

	TDS	eTDS	ERK score
Included	DIO1 DIO2 DUOX1 DUOX2 FOXE1 GLIS3 NKX2-1 PAX8 SLC26A4 SLC5A5 SLC5A8 TG THRA THRB TPO TSHR	BCL2 CDH16 CLCNKB DLG2 DPP6 FAM167A FHL1 FLRT1 GPM6A GRIN2C HGD KIT LMOD1 LRP2 MATN2 MPPED2 PKHD1L1 PLA2R1 SLC26A7 SLC4A4 SORBS2 STXBP5L TFCP2L1 TFF3 TPPP WSCD2 ZMAT4	ARID5A B4GALT6 BRIX1 BYSL CCND1 CD3EAP CHSY1 DDX21 DUSP4 DUSP6 EGR1 ELOVL6 ETV1 ETV4 ETV5 FOS FOSL1 GEMIN4 GTF2A1L GNL3 GPR3 GTPBP4 HMGA2 HYDIN IER3 KIR3DL2 LIF MAFF MAP2K3 MYC NOP16 PHLDA2 PLK3 POLR1C POLR3G PPAN PPAT PYCRL RRS1 SEMA6A SH2B3 SLC1A5 SLC4A7 SPRED2 SPRY2 SPRY4 TNC TNFRSF12A TSR1 WDR3 YRDC
Missing		LOC286002 MT1G	CXCL8

994